
Universiteit
Leiden
The Netherlands

A deep Westerbork survey of areas with multicolor Mayall 4 M plates. III - Photometry and spectroscopy of faint source identifications

Kron, R.G.; Koo, D.C.; Windhorst, R.A.

Citation
Kron, R. G., Koo, D. C., & Windhorst, R. A. (1985). A deep Westerbork survey of areas with multicolor Mayall 4 M plates. III - Photometry and spectroscopy of faint source identifications. *Astronomy And Astrophysics*, *146*, 38-58. Retrieved from https://hdl.handle.net/1887/7315

Version:	Not Applicable (or Unknown)
License:	Leiden University Non-exclusive license
Downloaded from:	https://hdl.handle.net/1887/7315

Note: To cite this publication please use the final published version (if applicable).

1985A&A...146...38K

Astron. Astrophys. 146, 38–58 (1985)

ASTRONOMY
AND
ASTROPHYSICS

A deep Westerbork survey of areas with multicolor Mayall 4 m plates

III. Photometry and spectroscopy of faint source identifications

R. G. Kron[1,⋆], D. C. Koo[2,⋆], and R. A. Windhorst[3,⋆,⋆⋆]

[1] Yerkes Observatory, University of Chicago, Williams Bay, WI 53191, USA
[2] Department of Terrestrial Magnetism, Carnegie Institution of Washington, 5241 Broad Branch Road-Northwest, Washington, DC 20015, USA
[3] Sterrewacht Leiden, P.O. Box 9513, 2300 RA Leiden, The Netherlands

Received May 29, accepted October 1, 1984

Summary. This paper provides optical photometry and some spectrophotometry for 171 identifications found in a sample of 302 weak radio sources observed at Westerbork (with $S_{1.4}>0.6$ mJy). Four-band photographic photometry from fine-grained Mayall prime focus plates is presented with photoelectric calibration. The morphology and environment of the radio source identifications are given. Low-resolution spectroscopy with the Kitt Peak 4 m Cryogenic Camera and with the McDonald 2.7 m IDS yielded about 60 redshifts for $V\lesssim 21.5$.

Two certain radio stars were found. The fraction of quasars at the mJy level is about 20% of all identifications.

An observational distinction is made between red and blue radio galaxies, which for $V\lesssim 18.5$ are exclusively giant ellipticals and spirals, respectively. For $18.5\lesssim V\lesssim 21.5$, giant ellipticals are also the dominant population, having high optical luminosities within a small dispersion ($\langle M_V\rangle \simeq -22.7\pm 0.5$ for $H_0=50\,\mathrm{km\,s^{-1}\,Mpc^{-1}}$) and radio powers close to or just below the break in the radio luminosity function. For $18.5\lesssim V\lesssim 21.5$, about one-third of the mJy radio galaxies are bluer than the giant ellipticals. They are not morphologically like the brighter spirals, but rather are a different class of peculiar (interacting, merging, or compact) galaxies. The giant elliptical galaxies are associated with the classical extended radio sources with linear sizes in the range 20–200 kpc. The blue radio galaxy population has intrinsically smaller radio sources with a somewhat wider spectral index distribution.

The magnitude-redshift diagram and color-redshift relations do *not* show strong evolutionary effects in the optical luminosity and color of the giant elliptical radio galaxies out to redshifts of 0.6.

The red galaxies persist as the dominant population of mJy radio sources down to the plate limit ($z\sim 0.8$). A population of very faint, blue, radio galaxies is also seen, possibly the high-redshift extension of the blue galaxy population seen at $V\lesssim 21.5$. Unidentified radio sources with $S_{1.4}>9$ mJy could be mainly distant giant ellipticals, but for $S_{1.4}<9$ mJy, they can also be members of the blue radio galaxy class.

The bivariate (radio-optical) flux density distribution is used to put constraints on the epoch-dependent radio luminosity function, which shows density-enhancement factors of up to 10 for $z\sim 0.7$.

Key words: radio sources: general – galaxies: radio – stars: radio radiation of – cosmology

1. Introduction

Over twenty-five years ago, a collaboration of radio and optical efforts led to the discovery of powerful radio galaxies. Since that time, a wealth of information has been obtained for these objects with a view towards understanding both the origin of the radio emission and the enhanced nuclear activity of these galaxies at high redshifts. The origin of the radio emission has been studied by detailed multifrequency observations of individual radio galaxies, mainly at low redshifts, and the population evolution of the radio sources has been investigated by statistical studies of large numbers of sources at cosmological distances. While numerous phenomena have been identified in these surveys, we still lack a comprehensive physical theory that satisfactorily describes the various properties of active nuclei.

The present paper aims to contribute to the empirical understanding of faint radio galaxies at cosmological distances. We intend to achieve this by photometric and spectroscopic measurements of the optical identifications of very weak radio sources found in a recent deep survey with the Westerbork Synthesis Radio Telescope (Windhorst et al., 1984, Paper I). Among 302 sources in the complete sample with $S_{1.4\,\mathrm{GHz}}\gtrsim 0.6$ mJy (5σ), 171 reliable optical identifications were found on deep, multicolor Mayall 4 m plates (Windhorst et al., 1984, Paper II). As in other surveys, optical data are needed for redshift determination or redshift estimation, from which the radio luminosity function, and its dependence on redshift and other parameters, may be derived. Also, they give information about the nature of these galaxies, anticipating that an important piece of the puzzle may be the connection between optical and radio properties.

⋆ Visiting astronomer, Kitt Peak National Observatory, which is operated by the Association of Universities for Research in Astronomy, Inc., under contract with the National Science Foundation

⋆⋆ Now at Mount Wilson and Las Campanas Observatories of the Carnegie Institution of Washington, 813 Santa Barbara Street, Pasadena, CA 91101-1292, USA

Send offprint requests to: R. A. Windhorst

© European Southern Observatory • Provided by the NASA Astrophysics Data System

1985A&A...146...38K

In Sect. 2 we present the optical data, consisting of four-band photometry, notes on morphology and environment, and some spectroscopic information. Section 3 discusses the characteristics of the radio galaxy sample by combining the optical and radio data in ways that enable the radio galaxies to be classified. For the giant elliptical class, it is investigated whether the data show evidence for evolution of the optical spectra. Section 4 discusses the quasars and the radio stars. In Sect. 5, the bivariate radio-optical flux density distribution is used to put constraints on the epoch-dependent radio luminosity function of weak radio galaxies. In an Appendix, we give results of spectroscopy for several additional objects obtained since the rest of the paper was prepared.

2. Observations

2.1. Plate scanning procedure

The 171 radio source identifications were photometered on the Mayall plates used in the identification procedure, taking the best plate in each band whenever we had more than one plate. Paper II contains a detailed discussion of the 4 m plate material and of the astrometric and identification procedure. Our four passbands, hereafter referred to as *UJFN*, correspond roughly to the photoelectric bands, U, B, $(V+R)/2$, and I_K, respectively.

The photometry was based upon PDS scans made at the Midwest Astronomical Data Reduction and Analysis Facility. For each plate, the list of (α, δ) coordinates for all optical identifications of Paper II was converted to (x, y) positions on the Mayall plates, using the astrometric procedure described in Paper II. An 80×80 raster with 20μ steps in both coordinates was scanned with the PDS microphotometer around the position of each optical candidate. At the scale of the 4 m prime focus this is equivalent to a square 30″ on a side (0.″37 pixels). Calibration stars were scanned in an identical way and in the same PDS run, as were the sensitometer spots. The photographic density mode was used throughout. Transformation to magnitudes is done in the calibration stage (Sect. 2.2).

The first step was to produce auxiliary pictures by juxtaposing, for each radio source position, the raster scans in each of the four bands. These merged pictures are reproduced as Fig. 1 for the objects discussed individually in this paper. Similar pictures are reproduced in Paper II for *all* identifications in the complete radio-optical sample. These were especially useful for the photometry of very faint objects, since in each case, the position needed to center the diaphragm could be best determined from the band in which the object appeared brightest.

Each 80×80 raster was displayed in turn on a Grinnell system. The image could then be handled with a joystick using interactive commands. Two cursors mark the corners of a rectangle of variable height and width which can be placed anywhere in the picture. In general, the rectangle is constructed to include the radio source identification and as much apparently empty sky as possible, without including any neighboring objects. The background is evaluated within the area of the rectangle, as are the x and y centroids of the image. The profile and growth curve for the light are then displayed, after which it is possible to override either the (x, y) centroids or the background or both. These options are important because the centroiding is often not accurate for very faint images and the growth curve at large radii is very sensitive to slight changes in the background. Thus the degree of flatness of growth curve at large radii is a powerful diagnostic of the quality of the background determination.

Once an apparently satisfactory measurement has been made, the total intensity, integrated over successive radii of 5, 10, and 20 pixels, is entered into a table. Sometimes part of the object intersected the boundaries of the rectangle. In this case, the algorithm for computation of the profile and growth curve reconstructs the missing light on the assumption of circular symmetry.

2.2. Photometric calibration

2.2.1. Relative calibration

For each plate a calibration curve was constructed in the form of a lookup table (measured density vs. relative intensity), using a spline fit to the modal sensitometer spot densities vs. the $\Delta \log I$ values for each combination of filter and emulsion, as recommended by the 1974 KPNO tables.

In all cases, the flux within a radius of 10 pixels (3.″7) was used as the standard measurement of apparent brightness for stellar images. Even on the plates with the worst seeing, only a small fraction ($<1\%$) of the light is outside this circle. The apparent brightness for each standard star was scaled according to the deviation of the local background from the mean background (in intensity units). This should, at least in a crude way, account for sensitivity variations, and it corrects for occasional intrusions of the guide probe, for instance. In general, it is not clear that such scaling is always correct, since density fluctuations may occur without sensitivity fluctuations. Experiments with and without such scaling (Koo, 1981; Koo and Kron, 1982) have not been conclusive: sometimes the scaling appears to lower the deviations of apparent brightnesses between plates, and sometimes it does not help, or may even produce larger deviations. Since the density variations over the plate can amount to 15%, this is a potentially important factor in the photometry. Random photometric errors will dominate for the faintest objects, of course. Figures 2a and 2b show a comparison of independent measurements of the same radio source identifications on *different* plates in the area of overlap. The agreement is good, and would probably have been worse if we had not scaled the brightness according to the level of the background.

2.2.2. Absolute calibration

The next step involves establishing the photometric zero points for each plate from the standard stars. In SA 57 and SA 68.1, there exists faint photoelectric photometry in the B and V bands from unpublished work by Baum and by Sandage. In SA 57 a few stars have photoelectric U magnitudes. The procedure for transformation of these standard-star *UBV* magnitudes into our *UJFN* system has been discussed at length in Kron and Chiu (1981), and Koo and Kron (1982). The relation between measured photographic and the transformed photoelectric magnitudes is linear to within $0^m.15$ spanning almost five magnitude, deviating at levels brighter then $B=18.5$ or $V=17.5$ due to saturation. For the fields SA 57 and SA 68.1, our zero points should be about as accurate as the uncertainty in the photoelectric values themselves, at least for the J and F bands. To calibrate SA 68.2, we have measured stars in the region of overlap with SA 68.1, so that SA 68.2 is on the same system as SA 68.1.

In the Lynx fields, a zero point in the B band comes from photometry by Usher and Mitchell (1982) of blue stars in SA 28. There are on average four stars with $B>18.5$ within each of the four 4 m fields. These objects are not ideal because some may be (variable) quasi-stellar objects, and in any case, they are so bright

© European Southern Observatory • Provided by the NASA Astrophysics Data System

1985A&A...146...38K

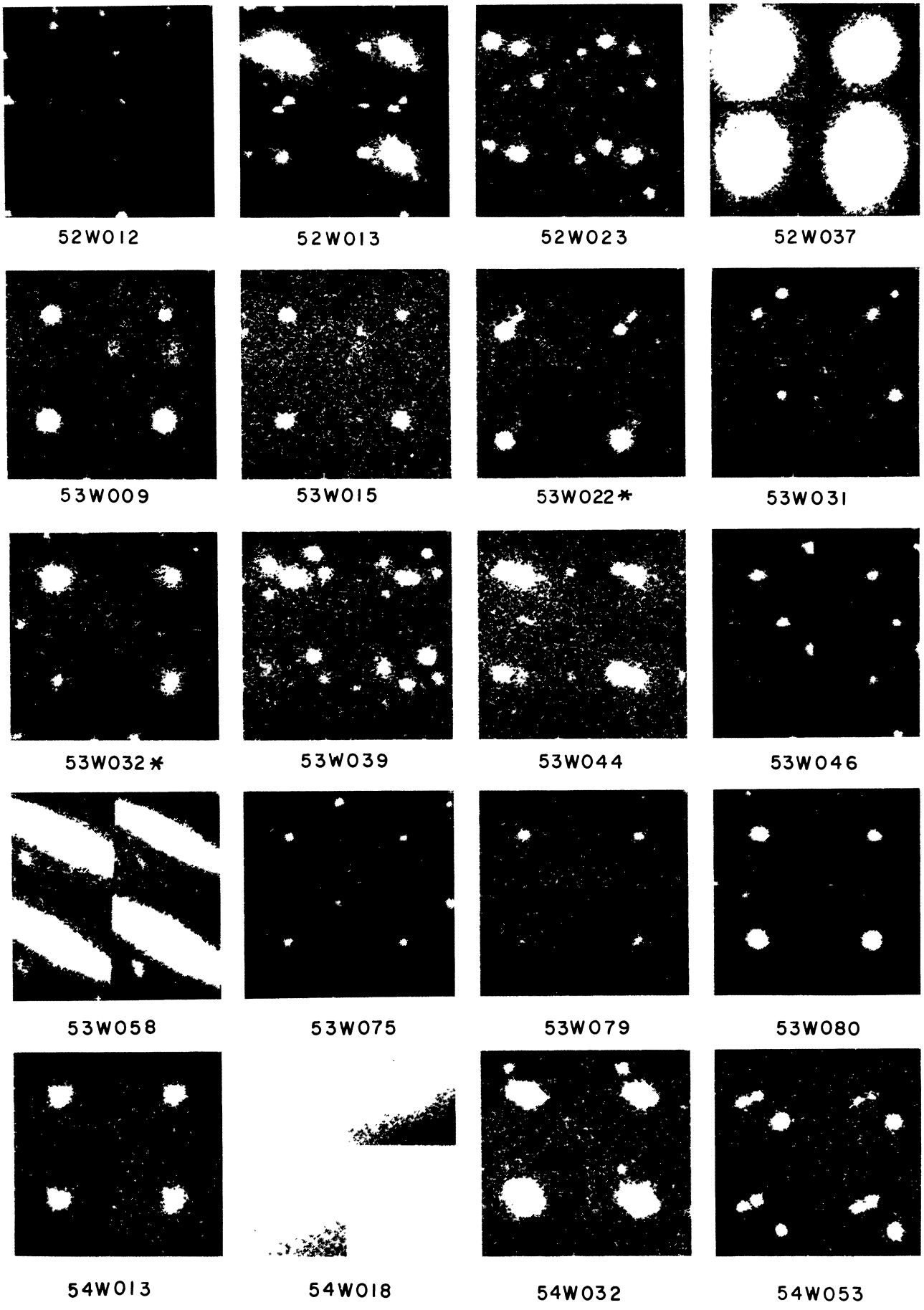

© European Southern Observatory • Provided by the NASA Astrophysics Data System

1985A&A...146...38K

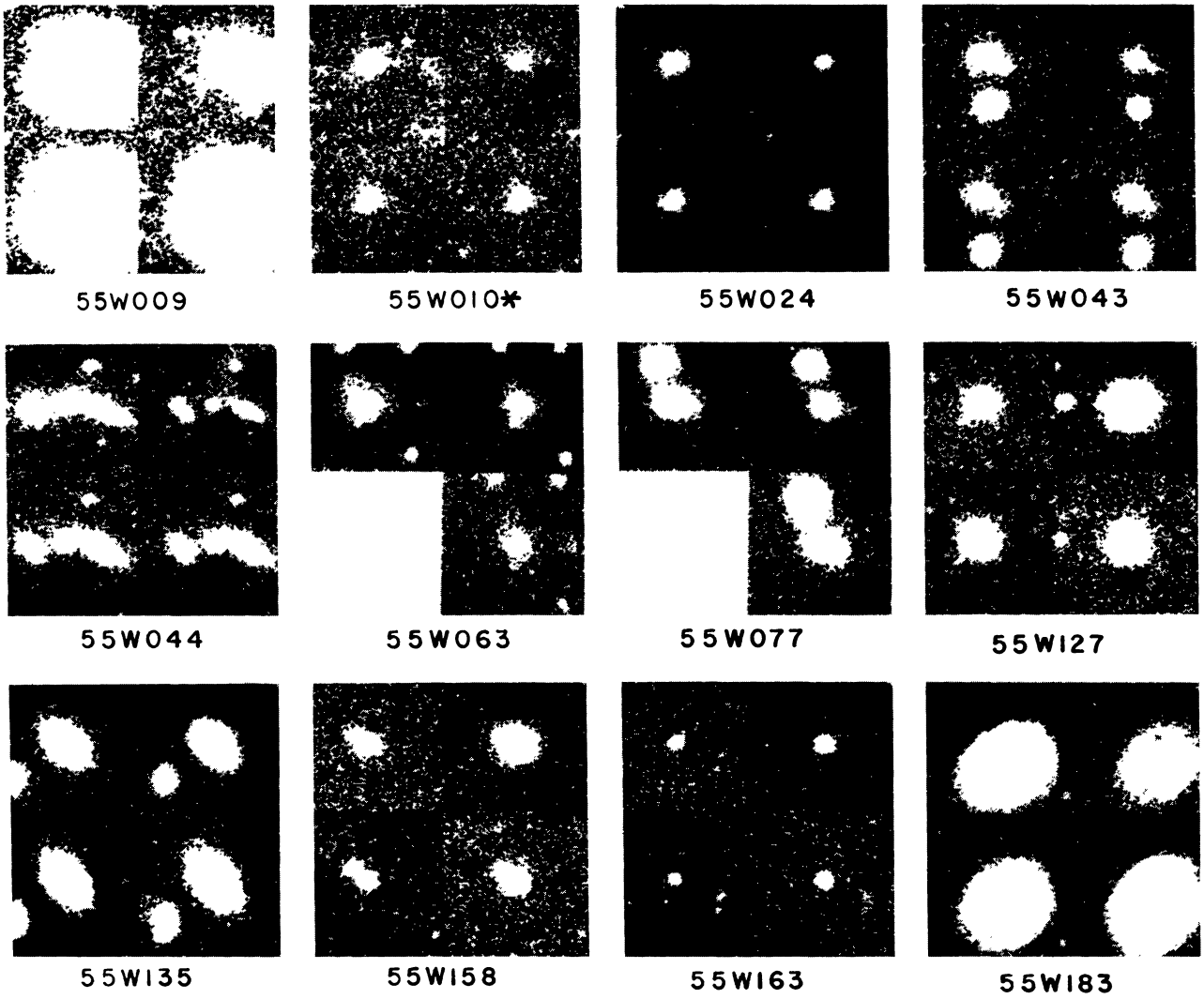

Fig. 1. Multiband images of the identified radio sources, in order of Westerbork number. Only for a limited number of radio sources photographs are given in this paper, namely for those objects that are discussed individually in the text. Photographs for *all* identifications in the complete radio sample are reproduced as Fig. 7 in the Supplements paper (Paper II)

For each object the U image is in the lower left, J in lower right, F in upper left and N in the upper right quadrant. The area around each image is 30″ on a side, except that the U and F image are cut off slightly at the left side. North is up, East is to the left. U data are lacking for Lynx 1 and Lynx 4 (the images appearing in the lower left of Lynx 4 objects are the J images repeated). The very limited dynamic range of these pictures must be kept in mind when evaluating galaxy morphology

that the linearity of the 4 m photometry cannot be taken for granted. In addition to the Usher and Mitchell objects, 18 "tie-in" or transfer stars were measured on each plate, which allows all four fields to be brought to a common magnitude scale. All instrumental magnitudes were first reduced to the system of Lynx 2. The B magnitudes for the Usher and Mitchell objects were transformed to J, assuming $B-V=0.5$, and then the J zero-point was derived from the grand total of 16 calibrating objects. The alternative of deriving a J zero-point for each of the fields separately, using just the few Usher and Mitchell objects in any given field, produces results which are completely consistent. The photometry of Usher and Mitchell (1982) is itself based on photometry by Sandage in SA 28, which is contained in our Lynx 2 field. Thus we have indirectly standardized on Sandage's system. We were able to check the derived zero point directly by the kind communication by Sandage of his unpublished work. We found good agreement ($\pm 0^m.1$), and no additional correction was deemed necessary.

No photoelectric calibration was available for the Hercules field, which will be dealt with as desribed below.

2.2.3. Color zero points

The next step is to provide the zero points for the bands other than J and F using the color distribution of the most common stars in the instrumental color-color diagrams. For the Lynx field, the procedure resembles that used in SA 57 and SA 68.1, except that now not only U and N need to be bootstrapped from model colors of typical faint stars, but also the F zero-point needs to be so determined. A star distribution model similar to that of Bahcall and Soneira (1980) was constructed to investigate whether substantial population differences would be expected between SA 57 and SA 68.1, and the lower latitude regions in Hercules and Lynx. These models predict that the faint spheroid stars at $B=21$ in Lynx and in Hercules, as in SA 68, are on average about $0^m.5$ more

© European Southern Observatory • Provided by the NASA Astrophysics Data System

1985A&A...146...38K

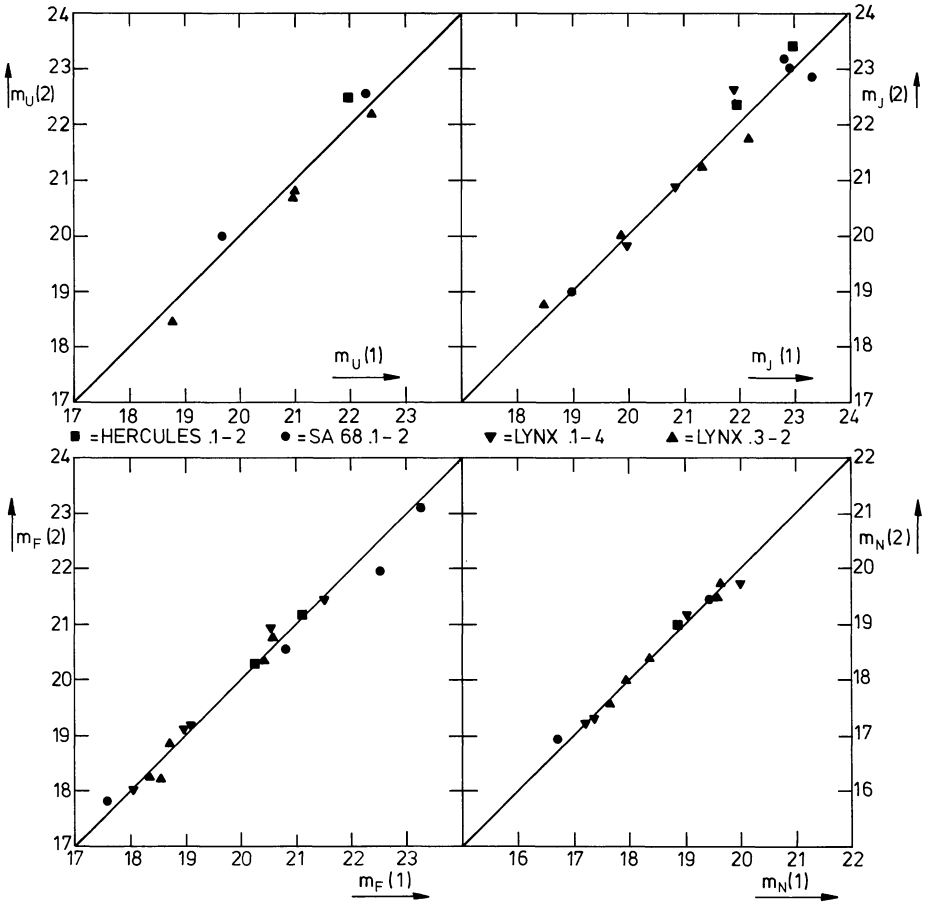

Fig. 2a. Comparison of photometry of objects measured independently in the overlap region of two plates. These objects are all near the edge, so the random errors would be overestimated from this comparison

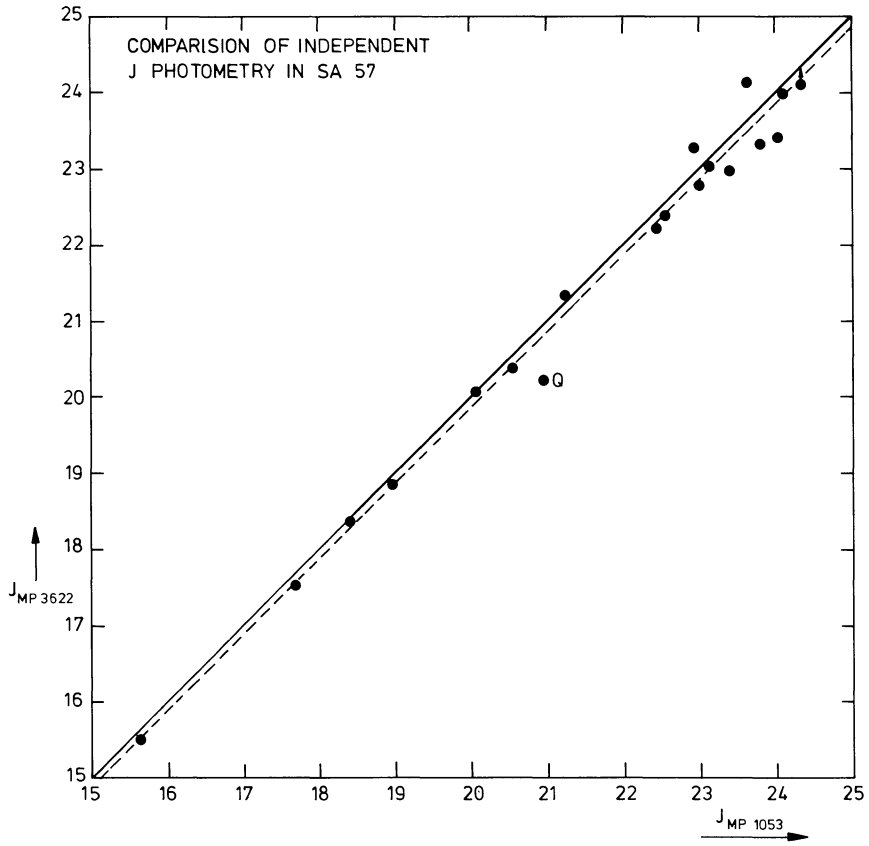

Fig. 2b. Comparison of photometry for objects on two *J* plates of SA57 (MPF1053 and MPF3266). Zero points were found independently from PDS scans of the standard stars on both plates. The quasar 52W047 is labeled *Q* and is evidently variable. The dashed line is a least-square regression, showing that the two zero points agree within $0^m.1$

© European Southern Observatory • Provided by the NASA Astrophysics Data System

1985A&A...146...38K

luminous than in SA 57, but as these are in the main-sequence turnoff and subgiant region, the difference in color is likely to be small. The distribution of absolute magnitudes for disk stars in Lynx is very close to that in SA 68. This distribution peaks about 1 mag brighter than in SA 57. In Hercules, the disk stars are brighter still by $0^m.5$ ($\langle M_B \rangle \sim +9$), but the dependence of $J-F$ color on absolute magnitude for these stars is weak. Combining all these uncertainties the estimated systematic error in the colors is $0^m.15$.

There remain the two fields in Hercules. The photometry for these two fields was tied together by measurements of 18 stars in common, and the procedure is similar to that described above for the Lynx field, except that no zero point in any band is available. Upon examination of the various zero points already established for plates with stars of known magnitude, it appears that an *estimate* may be obtained by assuming constancy of sensitivity of the plates. That is, after correcting for air mass differences, seeing, and exposure time, it is not unreasonable to expect a plate to have a zero point similar to another of the same emulsion, especially if taken during the same observing run. The error in this estimate is about $0^m.3$, but the color zero-points should be known to higher accuracy ($\lesssim 0^m.2$), because of the way they were established.

The final step is that of deciding on an appropriate measurement aperture for the identified objects. We have adopted a fixed aperture scheme, since most of the identified sources are small and faint. The default aperture is $7''.5$ in diameter, because $15''$ is so large that small errors in the background determination can become important, and $4''$ is generally so small that, except for stars, a non-negligible amount of light is outside that radius. To first order this would not matter for colors if the seeing were identical on all four plates of a field, but unfortunately, this is not the case. Thus, a circular area of $7''.5$ diameter seems to be a reasonable compromise. For the brighter galaxies ($F \lesssim 18$), a radius of 20 pixels was used in all bands, denoted by Table 1 by its diameter of $15''$. Occasionally, a radius of 5 pixels was used (denoted in Table 1 by $4''$) if some significant disturbance to the light (e.g. from a neighboring object) had occurred between 5 and 10 pixels radius in at least one of the bands. These special cases are without exception very faint objects. Sometimes the components of a double or double-nucleus galaxy were so close that both were unavoidably in the aperture, which is then noted in Table 1. Magnitudes are unreliable for objects near the edge of the 4 m plates, or which are in the guide-probe shadow on one of the plates. These cases are indicated by "edge" in Table 1.

No corrections for galactic absorption have been made to the magnitudes. The procedure for normalizing the color zero point to the expected unreddened colors of stars automatically takes out most of the reddening since the stars are, in general, beyond the dust. In any event, the reddenings in the fields are expected to be low, according to the Burstein and Heiles (1982) maps. The worst case is SA 68, for which we estimate $A_U = 0.15$, $A_J = 0.12$, $A_F = 0.08$, and $A_N = 0.05$. Any systematic error caused by ignoring absorption and reddening is small, compared to other uncertainties and with the size of the effects that we will be considering.

2.3. *Classification of the identifications*

2.3.1. Morphology

The separation of stellar and nonstellar images was done by eye. In difficult cases, preference is naturally given to classification from the plate with best seeing and/or best-exposed image. Uncertain cases are denoted as ? in Table 1, otherwise G? or Q? as appropriate if there is doubt. All objects which are *morphologically* stellar are denoted Q, regardless of color. The uncertainty in the classification is a function of apparent magnitude, and in individual cases errors in this classification may have been made. For instance, a distant elliptical galaxy can appear to be quite compact, and may therefore be classified as Q? or even Q. In this case, the colors should distinguish the object as a galaxy if it is not so faint that the color errors are large.

Within the class of objects classified as G, some degree of morphological information was attempted. We wanted maximum flexibility in order to cope with peculiar objects, and also a system that could be applied to moderately faint images. Our scheme crudely classifies according to apparent bulge-to-disk ratio for the brighter objects and notes the degree of concentration of light for the fainter objects. Type 1 is a pure bulge system like a giant elliptical galaxy. Type 2 has a disk, of which the prototype is M 104. Type 3 has a lower bulge-to-disk ratio, like M 31 or M 81. Type 4 is like M 51, and Type 5 has virtually no bulge, like M 33. For very faint galaxies, 1 means compact, 5 means diffuse, and 3 is intermediate. The error in the estimated bulge-to-disk ratio index is about ± 1 for bright galaxies and ± 2 for the fainter ones. Very faint galaxies may not have a morphological classification at all, in which case, for statistical purposes, G can be taken to correspond to Type 3, and G? to Type 1. In general, Type 1 galaxies have high surface brightness, and for Type 5, the opposite is the case. Exceptions are noted in the Comments in Table 1. This morphological scheme was set up to be independent of the colors, although correlations are to be expected in the sense that Types 4 and 5 will generally be bluer than Types 1 and 2.

2.3.2. Environment

In general, there is no easy and reliable way to tell if the objects near the radio source identification are physically associated. The best that can be done without an elaborate analysis of the radio source environments is to determine the subjective index that accounts for redshift in a qualitative way. Other than double galaxies (a pair within ~ 1 mag and ~ 1 image diameter of each other, denoted as DB in Table 1), we have only two environmental classes: group (GR), meaning that fewer than five galaxies within about two magnitudes are apparently associated with the radio source, and cluster (CL), meaning that if enough of the luminosity function were visible, the environment would probably turn out to be of Abell richness 0 or richer.

2.4. *Spectroscopy*

We have begun a spectroscopic investigation of the identified radio sources, and the results so far have been extremely important for the analysis (Sect. 3). At present, the reduction software is not fully developed for spectra obtained at Kitt Peak (see below), so only redshifts are listed in Table 1, and some are accurate to only about 0.01 in z. Future spectral reductions may provide information on absorption-line strengths, the presence and strengths of emission lines, the amplitudes of spectral discontinuities, etc.

Spectra for the brighter radio source identifications have been obtained at the McDonald Observatory with the Image Dissector Scanner (both blue and red chains) on the UVITS spectrograph of the 2.7 m telescope. The spectral range covered was usually 3600–6100 Å at ~ 10 Å resolution (gratings 2 and 7), but some spectra included also the red range (grating 5). A few of the more recent spectra were obtained at 15 Å resolution (grating 4). Apertures were $3'' \times 4''$, and because of this small size, no real effort

© European Southern Observatory • Provided by the NASA Astrophysics Data System

1985A&A...146...38K

was made to achieve high spectrophotometric precision (the photographic broadband colors are likely to give a more accurate representation of the continuum shape). As a rule, an integration was terminated as soon as a secure redshift was evident in the on-line display.

The fainter radio source identifications were observed at the Kitt Peak National Observatory with the CCD Cryogenic Camera on the 4 m telescope. This was done either with a slit of width 2.″5 or with an aperture plate mask in which one or more 2.″5 apertures correspond to the positions of radio source identifications within each 5′ diameter field. Grating prism No. 770 was used for all observations, giving a useful spectral range $\lambda\lambda$4800–7800, depending to some extent on where on the plate the aperture was located. The resolution with this setup is about 15 Å. We focussed to optimize the center of the detector, and as a consequence, the far red part of the spectra are generally badly defocussed. Nonetheless, sometimes the only strong feature was redshifted Hα in emission, which would have been missed altogether without the red sensitivity.

The slit was used for the brighter objects and the aperture plates for the fainter identifications. The other objects observed in these masks were a combination of faint field galaxies, selected only by F magnitude, and quasar candidates, selected by color. Some of the masks were constructed to contain as many radio sources and quasar candidates as possible within each 5′ field (the surface density of faint galaxies is so high that they are not a constraint), subject to the availability of nearby stars for positioning the mask. This procedure ensures that we also have spectra for objects in the angular vicinity of many of the radio source identifications, although objects very close to the radio source cannot be simultaneously observed because of geometrical constraints.

We have some hints of clustering (superclustering?) at high redshifts, regarding both coincidence in redshift among the radio source identifications themselves, and coincidence between the redshifts of the field galaxies and the radio sources.

A few redshifts have been obtained by H. Spinrad at Lick Observatory (3 m IDS) and by H. Butcher at Kitt Peak National Observatory (4 m Cryogenic Camera), which they have kindly made available to us.

The redshifts reported in this paper are only those in which we have high confidence, based on the visibility of at least two strong features. For galaxies with cold spectra, we used λ4000, the G band, and Mg b, while sometimes Na D was also visible. The emission lines used were $\lambda\lambda$4959, 5007, 3727, and the Balmer lines.

2.5. *The data*

The optical data and some radio data are given in Table 1a for the complete sample. Table 1b contains data for an additional list of objects which fail either the radio or the optical criteria for inclusion in the complete identification sample (see Papers I and II). For convenience we give an abbreviated tabulation of the relevant 21 and 50 cm data from Papers I and IV (Windhorst and Oppe, 1984), as well as of the identification data from Paper II. It must be stressed that the use of these data should be accompanied by a careful reading of these papers, especially regarding the notes on the reliability of the identifications in Paper II and the use of the weights that the sources should have in studies that depend on radio flux density (Paper I). Other information on radio variability and source morphology is also found in Papers I and II. The format of Tables 1a and 1b is as follows:

Column (1): Source name, consisting of the Westerbork survey number and source sequence number. An * denotes a multiple source, whose components are labeled A, B, and C.

Column (2): Image class – G = extended, Q = stellar, ? = uncertain, S = Galactic star.

Column (3): Estimated bulge-to-disk ratio index (explained in Sect. 2.3).

Column (4): Environment – CL = cluster, GR = group, DB = double (see Sect. 2.3).

Column (5): Redshift. For the radio galaxies 52W012, 53W031, 53W039, and 53W044, the redshifts have been measured by H. Butcher, and for 52W013 and 53W046, by H. Spinrad.

Columns (6)–(9): Apparent magnitudes in the passbands U, J, F, and N (aperture 7.″5).

Column (10): *Notes on the photometry:* 4″ = aperture for some faint objects; 15″ = aperture for bright objects; BOTH = two very close objects were unavoidably in the aperture; EDGE = at the plate edge or close to guide probe; EST = photometry was an eye-estimate; U, J, F, and/or N = these passbands were unreliable (mostly too faint).

Column (11): *Numerals* are notes concerning the *optical* object: 1 = stellar, but not blue; 2 = unusual surface brightness (mostly high surface brightness blue, but sometimes low surface brightness red object); 3 = close companion or optical jet; 4 = optically variable; 5 = double radio source with *also* a possible identification in one of the components (see Paper II); 6 = there are other individual notes given in Paper II (Table 4); 7 = X-ray source (Katgert et al., 1983). *Capitals* are notes concerning the *radio* morphology when relevant for the reliability of the optical identification: A = classical double; B = complex or head-tail source; C = radio source not in the galaxy nucleus, usually a star-formation region or supernova remnant in a spiral arm; D = low surface brightness radio source with spectroscopically confirmed candidate; E = like D, with a likely candidate, but without spectroscopy. Individual cases are discussed in Paper II.

Column (12): Likelihood ratio. When less than 2, the reason why this candidate is nevertheless a likely identification is given in Paper II [see also the capital notes in Column (11)].

Column (13): Weight that the radio source should have in the source counts or other studies that depend on radio flux density (Paper I, Sect. 6).

Column (14): Total flux density at 1412 MHz in mJy ($=10^{-29}$ W Hz^{-1} m^{-2}).

Column (15): Source resolution code – U = unresolved, R = resolved, E = extended/complex.

Column (16): Largest angular size in arcsec or a 1σ upper limit for U sources.

Column (17): 50–21 cm spectral index α ($S_\nu \propto \nu^{-\alpha}$), or if not detected at 50 cm, an upper limit in α is given, based upon a 3.75σ upper limit to the 50-cm flux. The 50-cm data are from Windhorst and Oppe (1984, Paper IV).

3. Discussion of the radio galaxies

3.1. *Strategy*

Nine basic observational parameters are available to study the nature of the identified radio sources. These are the radio morphology (angular size), the radio flux density, and spectral index; the optical morphology, optical magnitude, three colors, and redshift. The goal is to construct, from correlations among these nine parameters, a description of the faint radio galaxies

© European Southern Observatory • Provided by the NASA Astrophysics Data System

1985A&A...146...38K

Table 1a. The radio-optical complete sample

NAME	ID	BTD	ENVIR	Z	U	J	F	N	NOTES (PHOT)	NOTES (ID)	LR	WEIGHT	S1.4 (MJY)	RES	LAS (")	ALPHA (50/21)
52W005	G	1			23.92	23.18	21.44	19.71		E	0.09	1.06	7.75	U	<13.6	0.62
52W008	G		CL		22.15	22.32	21.92	20.08			117.87	1.00	20.49	R	16.5	-0.19
52W012	G	1	CL	0.400	22.01	23.10	22.11	21.94	U N		38.80	1.00	10.02	U	<10.5	1.14
52W013	G	1	CL	0.241	20.20	18.90	17.32	16.24	15"	6	88.10	1.96	2.88	U	<17.4	0.51
52W017	?				22.81	24.04	22.49	21.83			130.04	1.37	4.09	U	<22.1	0.49
52W020	G	3		0.060	18.08	17.59	16.53	15.78	15"		101.39	2.17	3.06	U	< 7.6	1.08
52W022	?				23.52	23.73	22.95				51.34	1.17	4.16	U	< 4.8	0.48
52W023	G	1	GR	0.202	19.55	20.05	19.65	18.86		D	0.00	17.93	1.22	U	< 7.7	1.47
52W034	G	3	GR		21.54	21.27	20.50	19.92			18.91	4.10	1.93	U	<14.9	1.54
52W037	G	4		0.023	15.61	15.58	15.14	14.44	15"	2	119.11	1.14	4.77	U	< 9.5	0.79
52W038	G				23.56	23.56	21.36	19.72		4	51.41	1.07	7.22	R	11.7	0.92
52W039	?						22.98	20.85			5.59	2.87	3.56	U	< 8.5	1.10
52W044	G	1		0.300	20.96	20.46	18.75	17.73	U		31.57	1.20	10.20	R	25.1	0.67
52W047	Q				19.43	20.58	20.76	19.67			234.73	1.00	38.07	U	< 2.2	0.42
53W005	G		GR			23.85	22.82	20.98			43.69	1.19	7.58	U	<16.6	1.09
53W008	Q		CL		20.47	20.87	20.21	19.41			153.41	1.00	306.60	R	6.5	0.79
53W009	Q			1.090	17.23	17.90	17.44	17.55			154.11	1.00	92.68	R	20.0	0.38
53W010	G	1			22.45	21.90	19.86	18.58			48.99	1.08	8.12	R	11.0	0.73
53W011	G	3	CL		21.49	22.13	20.72	19.96	BOTH		8.30	2.52	3.48	U	< 8.8	<-0.28
53W014	?		-		22.77	22.98					68.32	1.24	5.28	U	<15.7	<-0.81
53W015	Q				19.04	19.99	18.74	18.62			168.81	1.00	184.60	R	16.1	0.78
53W020	G	1	GR	0.100	19.12	18.32	17.03	16.26	15"		109.24	1.00	6.74	R	7.3	1.07
53W021	Q?		GR				22.32	20.76			24.90	1.18	4.71	U	< 9.9	1.07
53W022*	Q				17.80	18.00	17.40	17.95	EST	A	2.87	1.26	11.77	E	21.8	0.43
53W023	G	2			22.54	22.92	20.94	19.33			41.00	1.00	109.90	R	9.3	0.87
53W024	Q				19.87	20.90	20.70	19.89			38.59	1.00	10.33	U	< 7.3	0.55
53W025	?				22.88	23.56	22.68	20.99	U		36.31	16.09	1.14	U	< 8.7	< 1.03
53W026	G	1	GR		23.21	22.92	21.32	19.95			122.71	1.00	21.10	R	7.2	0.74
53W027*	G	3			22.79	23.08	22.00	20.91		B	10.64	2.35	8.25	E	26.8	0.80
53W029	Q				23.02	23.82	21.98	21.34	U		216.36	1.00	22.23	U	< 2.2	-0.23
53W030	G	1	DB		22.88	21.85	19.96	18.86	U		15.42	4.68	1.41	U	< 7.8	< 0.60
53W031	G	1		0.628		23.01	21.03	19.20			113.89	1.00	116.50	R	6.1	0.70
53W032*	G	2			20.91	20.45	18.88	18.01			3.61	1.24	10.48	E	22.4	0.80
53W034*	G	3			22.68	22.85	21.96	22.12	N	B	1.57	1.88	10.93	E	40.2	1.00
53W035	?				22.47	23.70	21.94	22.02	UJFN		164.86	1.46	4.39	R	7.3	-0.44
53W036	Q?				21.79	22.02	21.58	21.01			48.31	1.38	3.18	U	< 6.5	1.24
53W039	G	2	CL	0.402	22.35	21.30	19.23	18.12	BOTH		2.99	1.59	3.43	U	<11.4	0.82
53W044	G	2		0.311	21.45	20.67	18.90	17.82			30.06	5.10	1.75	U	< 8.5	0.92
53W045	G	1			22.22	21.17	19.29	18.16			32.62	7.17	1.48	U	< 9.0	< 0.58
53W046	G	2		0.545	22.24	22.17	20.27	18.94			18.69	1.10	63.10	R	2.1	0.69
53W047	G	1	DB		22.83	22.68	20.67	19.49	U		181.29	1.00	23.90	R	4.6	0.67
53W048	G	1				23.28	20.99	19.41			109.34	1.00	11.48	R	11.0	0.81
53W051	Q		GR		22.49	21.56	19.97	19.42	EDGE	E	0.0	1.00	141.60	R	19.6	0.87
53W052	G	1	GR		22.54	23.20	21.15	19.88	N	D	0.14	1.10	8.61	U	< 8.2	0.74
53W058	G	4		0.034	17.45	16.74	15.61	14.44	15"	C	0.0	8.87	1.39	U	<11.3	< 0.52
53W061	Q?					22.60	21.13	20.06			68.79	2.52	2.56	R	12.3	<-0.15
53W062	G	3	CL		22.54	23.16	21.39	19.89	U		29.17	7.33	1.74	U	<17.7	< 0.28
53W065	G	5			22.43	22.90	21.94				3.56	1.00	5.25	U	< 4.1	1.21
53W068	?				22.46	22.80	22.98	22.71	N		157.87	1.33	3.89	U	< 9.8	0.33
53W071	G	3		0.287	21.59	21.98	20.90	20.19			10.53	2.75	2.78	U	< 9.5	1.44
53W072	G	4		0.019	16.61	16.26	15.09	14.29	15"		30.78	1.39	6.56	U	<13.7	0.17
53W075	Q			2.150	21.60	22.15	20.81	19.49			212.16	1.00	96.13	U	< 1.2	0.78
53W076	G	1		0.390	22.93	21.75	19.45	18.28			43.27	6.69	1.42	U	< 9.4	< 0.89
53W077	G	2				23.85	21.46	19.93		B	0.0	1.54	7.78	R	16.8	0.87
53W078	G	2	GR		21.75	20.69	19.07	17.84			8.39	4.33	1.99	U	<16.1	< 0.53
53W079	G	1		0.548	23.21	22.59	20.76	19.21			67.22	1.00	13.25	R	8.4	0.05
53W080	Q		CL	0.546	17.91	18.26	18.25	17.56		D	0.52	1.00	27.59	R	11.0	0.80
53W083	G	5			22.68	23.14	22.02	20.26			175.63	1.01	5.02	U	< 5.3	0.70
53W085	Q			1.820	21.07	22.79	21.92	22.27	N		136.84	1.05	4.31	U	< 5.5	1.29
53W086	G	3				23.90	21.54	20.09		D	0.23	1.53	4.95	R	11.2	0.35
53W090	G	4		0.094	17.51	17.57	16.90	16.05	15"	2	18.68	4.13	2.06	U	< 9.3	< 0.83
54W008	G	5		0.015	15.00	14.75	14.00	13.50	EST	C	1.90	1.16	12.08	U	<99.0	
54W009*	G	1	GR	0.083	17.89	16.96	15.71	14.54	15"	7	4.23	1.52	5.99	E	22.5	
54W013	G	2		0.249	18.66	18.57	17.99	16.71		3	36.82	7.93	1.51	U	< 8.2	
54W014	?				22.89		22.03	20.74			40.21	1.10	5.47	U	< 5.5	
54W017*	G	1	CL	0.512	23.00	22.32	20.24	18.98			3.65	1.71	10.76	E	23.8	
54W018	G	4		0.038	18.50	17.90	17.08	16.37	15"	C	0.00	2.68	3.22	U	< 7.6	
54W021	G	2	GR		23.25	22.58	20.31	19.04	U		41.59	2.36	2.23	U	< 6.5	
54W028	G	2		0.173	19.86	18.99	17.71	16.82			67.96	1.10	53.30	R	15.3	
54W034	G	4			18.62	17.94	17.24	16.24	15"	C	0.13	2.64	2.10	U	<18.0	
54W036	G				21.30	22.30	21.27	20.04			17.18	1.16	5.72	U	<55.6	
54W038	G	2			22.92	22.98	20.69	19.51	U		94.06	1.20	5.25	U	< 5.5	
54W039	G						21.85	20.07			53.29	1.00	8.39	R	25.8	
54W048	Q				20.97	22.33	22.08	20.94			46.11	1.03	5.37	U	< 5.2	
54W049	G				23.11	23.06		20.95	F	E	0.10	1.51	5.68	U	<27.8	
54W050	G	3	CL		22.92	23.57	22.75	20.68			58.00	1.00	17.58	U	<24.8	
54W052	G				22.92	23.01	22.24				184.43	1.10	10.40	U	< 4.3	
54W053	G	4	DB	0.302	20.76	21.32	20.63	19.79		D	0.43	1.73	2.82	U	< 5.9	
54W057	G?				23.38	23.05	23.07	20.38	UJFN		154.94	1.00	476.60	R	8.8	
54W058	G	3				23.71	21.60	19.88			22.92	1.61	3.73	U	<26.2	
54W065	G		CL		23.17	23.46	23.06				5.42	2.03	2.55	U	< 6.5	
54W067	G				22.04	22.45	22.16	20.76			145.43	1.00	66.55	U	< 1.5	
54W068*	G		CL			24.20	22.57	20.35		5	33.54	1.00	24.61	E	33.4	
54W070	Q?				22.42	23.11	23.18		F	1	60.99	1.52	5.33	U	< 6.4	
54W071	?					23.40	22.28				22.21	1.44	5.41	U	<68.6	
54W072	G	4			20.58	20.11	19.10	18.02			5.00	3.27	2.77	U	<20.7	
54W073	Q		GR		19.19	19.61	19.23	19.01		7	28.72	3.01	2.70	U	< 8.0	
54W078	G	1	CL		24.34	21.50	19.52	18.55	U		2.28	1.10	10.42	R	20.5	
54W079	?					22.99					227.17	1.00	254.40	R	6.4	
54W081	G	3			20.78	20.92	19.87	19.05			176.49	1.00	15.02	U	< 3.4	
54W084*	G	1				22.08	19.92	18.66			11.92	1.00	28.55	E	15.6	
54W088	G	2			22.63	21.87	19.93	18.72	J		14.26	1.01	11.62	U	< 5.2	
55W007	G	1	CL				21.41	19.74			116.52	1.04	8.47	U	< 6.2	1.24
55W010*	G	2				20.31	19.15	17.82			75.31	1.00	32.76	U	<39.4	0.37
55W016	G	1				21.47	19.55	18.20			9.55	1.34	5.92	R	8.3	1.27
55W017	G	1				21.73	19.87	18.59			161.40	1.09	7.68	U	<11.5	0.70
55W018	Q					21.07	20.91	19.19	EDGE		79.06	1.00	34.59	U	< 9.8	0.61
55W019	G	1	GR			22.41	20.52	18.93			144.71	1.48	4.16	U	< 7.7	0.20
55W020	G	5		0.040		15.68	14.72	14.09	15"		28.65	7.09	2.37	U	<15.2	1.10
55W023	G	1	GR			20.65	18.96	17.63		E	0.03	3.31	4.07	R	11.5	0.42
55W024	G	2				20.57	19.10	17.93			102.44	1.29	4.85	U	< 7.4	0.71
55W027	G	3				22.93	22.07	21.11			72.88	7.14	1.83	U	< 8.0	1.37
55W034	G					23.16	22.76		EDGE		69.46	3.47	4.19	U	<10.8	<-0.16
55W036	G	4				21.96	20.41	18.70			142.25	1.03	6.29	U	< 4.6	0.61
55W037*	G	1		0.210		18.81	17.32	16.32	15"	A	0.02	1.00	1519.20	E	114.2	0.76
55W041	G	1		0.080		17.02	15.77	15.01	15"	D	0.05	5.59	2.02	U	< 8.6	< 0.12
55W042	G	4	CL			23.59	21.56	18.94			71.43	1.02	12.27	U	< 9.9	1.08
55W043	G	2				20.22	18.49	17.34		E	0.57	1.13	8.27	R	8.8	0.93
55W044	G	1	CL			20.67	19.15	18.15		E	0.0	1.00	15.80	R	11.7	0.90
55W046	G						22.77	20.36			50.07	1.15	9.91	U	<10.4	0.90
55W049	G	3	CL			22.29	20.76	19.12	EDGE		48.31	2.27	4.52	U	<10.1	-0.44
55W056	G	2				20.87	19.05	17.87			21.68	1.07	6.74	U	< 6.5	-0.51
55W058	G	3	GR			22.91	21.04	19.38		R	0.03	1.61	4.25	R	14.6	0.92
55W063	G	1	CL			19.90	18.02	17.21	15"		165.46	1.00	24.50	R	7.2	0.46

© European Southern Observatory • Provided by the NASA Astrophysics Data System

© European Southern Observatory • Provided by the NASA Astrophysics Data System

Table 1a (continued)

NAME	ID	BTD	ENVIR	Z	U	J	F	N	NOTES (PHOT)	NOTES (ID)	LR	WEIGHT	S1.4 (MJY)	RES	LAS (")	ALPHA (50/21)
55W065	G?						21.79	19.18			83.66	2.05	2.72	U	<13.4	0.28
55W066	G	1				22.46	21.18	19.75			19.13	1.00	24.70	R	10.4	0.73
55W067	G					23.50	21.49	19.86	J	1	351.39	1.00	9.82	R	8.1	0.37
55W068	G	2				22.26	20.34	19.27			141.39	1.34	3.56	U	<13.1	1.38
55W070*	Q					22.31	20.65	17.92		A	0.0	1.07	11.18	E	37.5	1.18
55W075	Q					21.26	20.85	19.33			312.68	1.00	187.30	U	< 1.0	-0.96
55W077	G	2	DB	0.126		18.38	17.47	16.72			270.37	1.00	8.75	U	< 4.6	0.59
55W080	?					23.62		20.54		B	0.0	1.00	9.66	R	23.5	0.78
55W092	G	2				22.90	20.83	19.18			26.70	2.27	2.48	U	<17.6	1.27
55W093	G?						21.63	20.35		E	0.13	4.62	1.46	U	<12.4	0.84
55W097	G?		CL			21.23	19.86	19.04			6.13	15.09	0.91	U	<11.4	< 1.32
55W102	G?	3				22.95	23.00				254.62	1.00	9.66	U	< 7.8	1.09
55W105	G	2				18.73	17.47	16.73	15"		111.50	1.46	3.94	U	< 9.5	0.51
55W110*	Q			1.780	18.05	18.76	18.27	17.56			97.51	1.10	24.80	E	47.9	0.87
55W111	?		GR			23.72		20.41			91.79	1.05	6.30	R	14.3	-0.64
55W116	G	3					21.81	20.61			4.60	5.01	0.96	U	< 9.3	< 1.25
55W118	Q					22.57	21.12	20.23		1	0.04	5.21	1.00	U	<12.5	< 1.14
55W121	Q				22.30	22.66	22.99				83.21	4.09	1.04	U	< 9.5	< 0.98
55W124	Q				21.74	21.21	21.17	21.38			215.21	1.00	5.21	U	< 6.4	-0.25
55W125	Q?				22.66	23.21	22.44	21.01			14.95	1.00	21.36	R	8.3	0.24
55W127	S				15.89	16.02	15.64	13.82			57.13	1.91	1.31	U	< 6.9	1.44
55W129	G	1			22.88	22.11	20.03	18.73			61.42	16.15	0.57	U	<10.0	< 1.55
55W135	G	4		0.089	17.15	17.11	16.25	15.45	15"		176.49	1.18	2.38	U	< 5.9	0.68
55W137	G	3		0.160	18.82	18.70	17.80	17.00	EST	6	125.71	1.54	1.60	U	< 6.1	1.72
55W144	G		DB		21.13	21.40	20.38	19.61	BOTH		59.06	1.59	2.68	U	<10.1	0.57
55W149	G	1	GR	0.150	18.86	17.96	16.52	15.66	15"		215.51	1.00	6.98	R	8.5	0.84
55W150	G	1	CL		22.49	22.11	20.73	19.42	BOTH		85.78	6.83	0.84	U	< 9.3	< 1.08
55W153	?					23.16	22.33				7.19	2.34	1.94	R	11.9	1.49
55W154	G	1	CL		22.17	21.21	19.61	18.42			14.79	1.00	11.70	R	15.0	0.73
55W157	Q				22.61	22.94	22.11	21.14	4"		86.87	2.72	1.23	U	<10.5	< 0.46
55W158	G	3			20.80	21.50	20.35	19.60	EST		2.78	10.36	0.69	U	< 9.4	< 1.04
55W160	?				22.95		22.08	20.71			4.38	6.75	0.85	U	< 9.6	0.76
55W161*	G	1			22.85	21.86	20.05	18.73		5	4.45	3.54	3.20	E	48.9	1.50
55W163	Q				20.90	19.95	18.80	17.98		6	14.14	2.98	1.97	U	< 8.8	-0.19
55W164	Q				22.31	22.92	22.13				5.59	10.82	0.67	U	<10.3	< 1.05
55W165*	Q?				22.82	23.55	22.14	21.24		5	6.98	1.00	17.60	E	37.9	0.82
55W166	G	3			23.33		21.96	20.11			164.38	1.30	2.40	U	<12.6	0.89
55W171	G	1			22.29	21.97	20.68	19.51			208.83	1.25	2.89	U	< 6.8	-0.09
55W173	Q				20.82	21.28	20.40	19.68			190.70	1.15	3.57	U	< 6.5	0.93
55W175	G	1	GR		21.78	22.60	21.74	21.30			189.82	1.00	42.90	U	< 2.4	-0.48
55W178	G	5		0.041	16.39	16.41	15.49	14.86	15"		58.42	4.52	1.24	U	<12.8	1.41
55W179	Q				18.59	19.06	18.41	18.37			113.00	1.00	4.98	U	< 4.0	0.61
55W183	G	6		0.088	19.75	19.96	19.32	18.64		C	36.95	5.62	1.33	U	<13.8	< 0.27
55W184	G?				23.05	23.26	21.92	21.41			61.16	6.84	1.07	U	<16.8	< 0.53
55W187*	G	2			23.07	21.46	19.67	18.31		A	8.79	1.00	19.29	E	36.8	0.72
55W188	G?					23.49	22.13	19.71		1	134.79	1.00	12.10	U	< 4.6	0.72
55W189	Q?					23.25	22.43	20.09			4.60	1.25	4.24	U	<21.3	<-0.58
55W190	G?		GR			22.91	20.91	19.50			128.46	1.00	11.00	U	< 2.5	0.56
55W191	G	4	CL		22.65	22.87	21.68	21.08	4"	3	7.64	1.00	13.99	U	< 3.7	0.63
55W198	Q?					23.07	21.18	19.51		1	100.54	19.90	0.58	U	< 9.8	< 1.42
55W199	G?	3			23.98	23.14	22.40	21.55			45.39	1.12	3.36	R	6.1	0.81
55W200	G	1			23.30	21.35	19.47	18.17			14.74	1.02	4.64	U	<11.2	0.37
55W209*	G	1	CL		22.76	22.33	20.31	19.10	BOTH	B	94.15	1.00	17.19	E	36.8	0.87
55W210	G	2	CL			23.35	20.87	19.17			31.97	1.77	2.58	R	9.5	0.53
55W222*	Q?	1			23.38	22.25	20.03	18.61		E	0.44	1.38	4.70	E	23.3	<-0.36
55W224*	Q				21.83	22.55	21.79				14.79	1.00	33.81	E	31.1	0.73
55W226	G	2			21.71	22.32	20.83	19.04			48.18	1.00	6.35	U	< 9.6	0.58

Table 1b. List of additional objects *not* in a complete sample

NAME	ID	BTD	ENVIR	Z	U	J	F	N	NOTES (PHOT)	NOTES (ID)	LR	WEIGHT	S1.4 (MJY)	RES	LAS (")	ALPHA (50/21)
52W009	Q?				21.95	22.46	21.47	19.85			12.29	0.0	2.84	U	<12.9	<-0.41
52W029	?						22.99				87.07	1.00	104.80	R	6.0	0.81
52W036	G	5	DB	0.240	18.18	18.37	17.38	16.63	15"	C	46.86	0.0	1.03	U	< 8.8	1.20
52W042A	?						23.52	20.49	FN	5	111.28	1.00	26.50		11.0	0.98
52W046	?				24.26	23.88					5.94	4.59	2.12	U	< 8.3	0.60
52W052	Q				22.04	22.88	22.40		N		4.23	0.0	6.45	U	<30.9	<-1.28
53W003	G	4	DB	0.050	16.79	16.95	16.09	15.74	15"	C	1.88	0.0	3.19	U	<20.1	0.38
53W028	G	2			22.74	21.12	19.02	18.17	U		35.71	0.0	2.65	U	< 9.4	< 0.63
53W067	?					23.58	23.00	21.19	JFN		36.34	1.00	23.20	R	10.4	0.81
54W005*	G?					19.07		16.13	EDGE		7.29	0.0	26.65	E	20.0	
54W025	Q?				20.36	21.11	20.84	19.31	EDGE		6.82	0.0	44.73	R	23.1	
54W032	G	3		0.097	15.46	16.55	16.24	15.17	15"	2	1.58	0.0	8.75	U	<44.6	
54W040	?				23.96				U		21.24	5.29	1.90	U	<18.2	
54W044	Q				21.59	22.54	21.86	21.10			8.93	0.0	1.71	U	<11.0	
54W047	Q				23.29	22.48	21.21	20.20			14.11	0.0	1.28	U	< 8.5	
54W056	G	1	GR		22.50	23.00	22.00		EST		1.60	0.0	2.53	U	<15.3	
54W059	?				23.31	24.11					2.14	4.46	1.75	U	< 7.3	
54W068A	G?		CL			23.77	22.33	20.82		5	1.41	1.00	14.81		21.6	
54W068B	G	4	CL		22.86	22.14	21.63			5	11.33	1.02	9.70		99.0	
54W069	?				23.93				U		4.51	1.08	5.23	U	< 5.6	
54W089	Q				19.36		20.27	19.79	EDGE		45.73	0.0	13.39	U	< 6.2	
55W009	G	5		0.050		19.77	20.21	19.29		C	38.11	0.0	2.84	U	<11.9	< 0.29
55W014	?		CL			24.82	22.40		JF		15.44	6.45	1.89	U	< 9.6	0.25
55W037A	?					24.73	23.04			5	14.97	1.00	703.30		29.1	0.41
55W037B	?					22.65	21.93	20.10		5	0.0	1.00	804.90		43.0	1.02
55W052	G	3				23.33	21.04	19.18			7.82	0.0	2.06	U	<15.4	0.47
55W074	Q					21.64	21.09				12.24	0.0	1.18	U	<22.6	< 0.78
55W096	?					22.96	22.47	21.44			4.33	0.0	0.95	U	<13.1	< 1.21
55W131	?							21.53			27.86	8.32	0.80	U	< 8.9	1.56
55W136	?		CL								35.64	7.55	0.77	U	< 8.3	1.60
55W152	G	4			19.00	18.50	17.50	16.50	EST		0.0	0.0	2.16	U	<15.9	0.72
55W161A	Q				21.53	21.76	21.36	21.42		5	0.0	1.71	1.96	R	19.0	2.05
55W161B	G	1			22.85	21.86	20.05	18.73		5	4.31	1.29	1.79	R	11.0	1.59
55W165A	?	3			23.62	23.57	22.40	21.44	4"	5	9.87	1.00	8.28	R	22.6	0.42
55W165B	?				23.01	23.57				5	0.0	1.00	9.48	R	14.1	1.07
55W168	G?	3				23.86	23.19	20.69	4"		43.15	0.0	1.45	U	<13.3	1.37
55W177	?				24.13	23.62	22.88				223.86	1.00	30.61	U	< 2.8	-0.33
55W202	?				23.15	23.90					18.60	10.71	0.76	U	< 8.6	< 1.12
55W205	?		CL				22.80	20.64			47.56	6.02	1.12	U	<12.5	0.65
55W206	G?				23.05	23.22	22.14	20.84	4"		6.65	0.0	2.26	U	<13.5	< 0.30
55W207	G	4	GR		20.80	21.67	20.90	20.12			1.70	0.0	2.12	U	<10.7	< 0.13

Notes to Table 1

52W012: Measured z is possible of another nearby object.
54W013: Read $F = 17.79$ instead of 17.99, also in the figures.
54W018: F is probably too faint because object is at the plate edge.
55W183: Only the magnitudes of the knot in the spiral arm are listed, not of the whole galaxy. Object is thus not plotted in the figures

1985A&A...146...38K

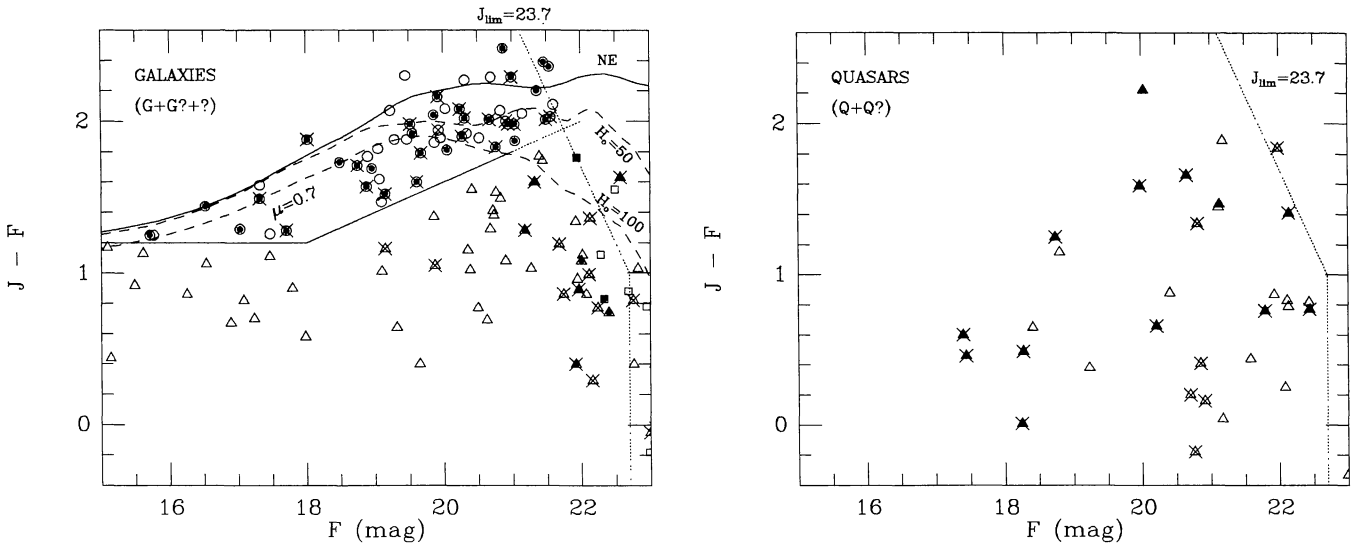

Fig. 3a. $J-F$ color vs. F magnitude for radio galaxies in the complete radio-optical sample. Squares are for objects of class ? in Table 1a. The classes G and G? are plotted as circles (red galaxies) and triangles (blue galaxies). The full-drawn line separating these two classes is given by Eq. (1). Sources which are resolved at 21 cm (HPBW = 12″) are marked by an interior-filled circle. Sources stronger that $S_{1.4}=9$ mJy have a superimposed cross. The top solid curve is the predicted color-magnitude relation according to Bruzual (1983) for a *nonevolving* gE with $M_F=-23.3$, $H_0=50\,\mathrm{km\,s^{-1}\,Mpc^{-1}}$, $q_0=0$, and current galaxy-age = 16 Gyr. The upper dashed curve is a mildly evolving elliptical spectrum with similar parameters to fix the relation between time and redshift. Other parameters are the slope of the (Salpeter) initial mass function, $x=1.35$, and the fractional galaxy mass that is processed into stars during the first Gyr, $\mu=0.7$. The lower dashed curve is a model for $H_0=100\,\mathrm{km\,s^{-1}\,Mpc^{-1}}$, $q_0=0$, age = 9 Gyr at $z=0$, and $M_F=-21.8$. Estimated completeness limits are $F=22.7$, $J=23.7$ (dotted lines). **b** $J-F$ vs. F magnitude for quasars (Q and Q?) in the complete optical-radio sample. Some of the red objects could be misclassified distant gE galaxies. Interior filled circles denote radio sources that are resolved at the 12″ beam and a cross denotes radio sources with $S_{1.4}>9$ mJy

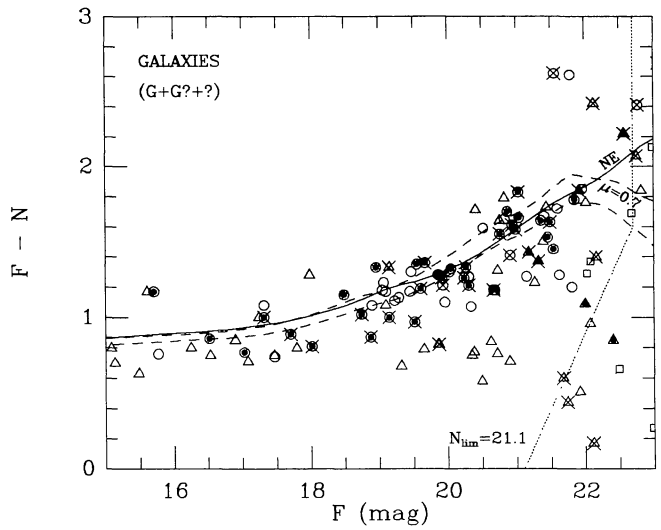

Fig. 3c. $F-N$ color vs. F magnitude diagram for classes G, G?, and ? in the optical-radio complete sample. The symbols and models are as in Fig. 3a

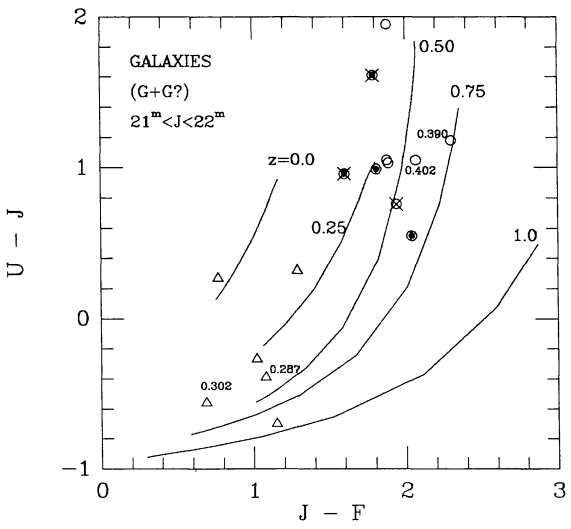

Fig. 4. $U-J$ color vs. $J-F$ color diagram for all galaxies with $21\leqq J<22$. Four of these have redshifts, as marked. The lines are loci of equal redshift for galaxy models with $0.01<\mu<0.9$ and for $H_0=50\,\mathrm{km\,s^{-1}\,Mpc^{-1}}$, $q_0=0$, and galaxy age = 16 Gyr at $z=0$. Symbols are as in Fig. 3a

without a priori assumptions. Once their nature has been determined, conclusions about evolutionary processes may be attempted. A full exploration of this nine-dimensional space is impractical with limited statistics. We will instead concentrate upon a subset of the possible combinations that best distinguish between the different classes of objects.

One important combination is the color-magnitude diagram for the radio galaxies (cf. Fig. 3a), of which $J-F$ vs. F is the basic one in the following discussions. The $J-F$ color is especially useful because of its overall quality and availability in all of our fields, and the F magnitude is plotted as the abscissa since virtually all identifications are visible in at least the F band (see the magnitude distributions of Paper II). There appears to be a division of faint radio galaxies between a red group near $J-F\sim2$ and a bluer group in the general range $0.6\lesssim J-F\lesssim1.6$. These two groups correspond closely to the morphological indes, based on the degree of concentration of light (Sect. 2.3), in the sense that Types 1 and 2 are red and Types 3–5 are blue. Furthermore, all bright ($F<18^m$) radio galaxies bluer than $J-F=1.2$ have spiral morphology and all bright galaxies redder that that are ellipticals. (Note

© European Southern Observatory • Provided by the NASA Astrophysics Data System

1985A&A...146...38K

that magnitudes and colors for very bright galaxies are likely to be inaccurate, because large galaxies overfill the 30″ frame, but for the present purpose all we require are relative colors.) At fainter magnitudes, $F>18$, a precise morphological distinction between red and blue galaxies is not possible, but down to $F=21$ high-surface-brightness red galaxies can still be distinguished from low-surface-brightness blue galaxies. The resulting division line (the solid slanted line in Fig. 3a) becomes redder with fainter magnitude due to the K-corrections. For $F>21$ even surface brightness is no longer a reliable discriminant, so we adopt an extrapolation of the slanted line (dashed line). Figure 3a shows that there are few objects with $F>21$ and $J-F\sim 1.8$, so that if the division should have occurred at somewhat bluer colors, only up to 6 objects in the complete sample would have been misclassified. The blue and red galaxy classes described above are *defined* by the regions in Fig. 3a occupied by triangles and circles respectively. The same symbols refer to these blue and red galaxies in all other figures. The separation between the two radio galaxy classes was taken as:

$$(J-F)=1.2 \quad \text{for} \quad F<18\,,$$
$$\text{and} \qquad (1)$$
$$(J-F)=0.2F-2.4 \quad \text{for} \quad F\geqq 18$$

indicated by the full-drawn lines in Fig. 3a. We shall refer to these groups as B and R galaxies, although it remains to be seen whether the faint representatives of these groups really belong to the same physical class as the bright ones (see Sects. 3.2 and 3.3).

In the following discussions, we will frequently refer to the radio data, which appear in various aspects of the discussion. Details of the selection and completeness of the radio sample are given in Paper I. We emphasize here that the faintest radio sources can only be seen over a small part of the survey area. However, under the assumption of isotropy within the WSRT primary beam, one can calculate how many other sources are represented by one detected faint radio source (Paper I). This is incorporated in the weights in Table 1. Two other properties of the radio survey are important. The 2σ criterion used to decide whether a radio source is resolved with the WSRT beam (HPBW $=12''$) is dependent on signal-to-noise ratio in the sense that stronger sources are more easily recognized as resolved. Also, since the flux errors are inversely proportional to the signal-to-noise ratio, larger errors are expected in the spectral index for fainter radio sources (up to 0.2–0.3 in α, Paper IV).

In Fig. 3a, the symbols have been coded according to radio information. Interior-filled circles denote a radio source that is resolved by the 21-cm WSRT beam, and crosses denote "strong" radio sources ($S_{1.4}>9$ mJy). For $F<21.5$, virtually all radio sources brighter than $S_{1.4}=9$ mJy, and all radio sources that are resolved with the 12″ beam, are associated with red galaxies. Conversely, essentially all blue radio galaxies with $F<21.5$ are fainter than 9 mJy and are unresolved radio sources.

Figure 3b gives the $J-F$ vs. F distribution for the stellar objects. About half of them are brighter than $S_{1.4}=9$ mJy. About one-third of them are also resolved in the 12″ beam, i.e., a smaller fraction than for the red galaxies. As remarked in Sect. 2.3, some of the redder, faint, nominally stellar objects could be misclassified galaxies. On the other hand, some of the fainter, blue, nominally extended objects could be misclassified quasars. For instance, there is a group apparent in Fig. 3a at $F\sim 22$ and $J-F\sim 0.9$ with radio properties more resembling those of quasars than the brighter blue galaxies. The properties of the stellar objects are discussed in Sect. 4.

In the following discussion, the objects can be naturally divided into three groups, according to optical brightness:

(a) Bright ($F\lesssim 18$) objects, for which morphological classification of galaxies is feasible, photometry is adequate, redshift determination is complete, and expected evolution is small.

(b) Faint ($18\lesssim F\lesssim 21.5$) objects, for which both the photometry and star/galaxy separation are accurate, the redshift sample is large and deep enough to calibrate colors to $z\sim 0.5$, and an overlap still exists with previous work.

(c) Very faint ($F>21.5$) objects, for which virtually no redshifts are available and for which the color errors and incompleteness increase rapidly at the plate limit, although magnitude and color information are still crudely reliable. Formally, we also include in this group the unidentified radio sources, whose properties can be deduced only by extrapolation of the radio and optical properties at brighter limits.

3.2. *Bright radio galaxies* ($F<18$)

The radio galaxies brighter than $F=18$ consist of giant elliptical galaxies and disk galaxies, the latter having a variety of forms. Their $J-F$ colors are consistent with those expected for nearby galaxies of these two categories.

3.2.1. Giant ellipticals

As a class, the bright red radio galaxies (see Fig. 5) follow a Hubble relation that is typical for powerful radio galaxies (Sandage, 1973). Their radio powers are given in Table 2 and are in the range $23\lesssim \log P_{1.4}/\mathrm{W\,Hz^{-1}}\lesssim 26.5$, with $\langle \log P_{1.4}\rangle \sim 24.1\pm 1.3$. Their absolute magnitudes were calculated using Bruzual's (1981) K-corrections (for $H_0=50\,\mathrm{km\,s^{-1}\,Mpc^{-1}}$, $q_0=0$ and galaxy age $=16$ Gyr) to be $\langle M_F\rangle \sim -23^{\mathrm{m}}.0\pm 0^{\mathrm{m}}.6$. This value may be compared to Sandage's value of $\langle M_F\rangle \sim -23.8$.

The radio-to-optical spectral index is obtained from:

$$\alpha_{\mathrm{ro}}=\log(S_{1.4}/S_F)/\log(21.2\,\mathrm{cm}/6100\,\text{Å})\,,$$
$$\text{with} \qquad (2)$$
$$\log(S_F/\mathrm{Jy})=-0.4(m_F-8.72)\,.$$

For red galaxies, this ratio is on average $\langle \alpha_{\mathrm{ro}}\rangle \sim 0.35$, or a monochromatic radio-to-optical flux ratio of $\sim 10^2$ (see also Fig. 8a to be discussed in Sect. 5).

As shown in Fig. 3a and Table 2, a considerable fraction of the red radio galaxies is associated with a radio source that is resolved with the 12″ WSRT beam. Their angular sizes were determined in Paper I and their linear sizes are generally in the range 20–200 kpc, with a median of about 60 kpc.

3.2.2. Spiral galaxies

The properties of the spiral radio galaxies are summarized in Table 3. For our bright spiral galaxy sample, with one exception, all radio fluxes are less than 7 mJy. Using Bruzual's K-corrections, the mean spiral galaxy absolute magnitude is $\langle M_F\rangle \simeq -21.1\pm 0.7$, close to that of a random field sample, and near the break in the optical luminosity function ($M_F^*\simeq -21.8$). The radio powers of the bright spiral galaxies are in the rather narrow range $21.9<\log P_{1.4}<22.3$, with $\langle \log P_{1.4}\rangle \sim 22.1\pm 0.1$, close to the break of the spiral radio luminosity function of Hummel (1980). Their average radio-to-optical spectral index is $\langle \alpha_{\mathrm{ro}}\rangle \sim 0.0$.

For 55W183 and 55W009, and possibly also for 53W058 and 54W018, the radio source positions coincided with the arms of

© European Southern Observatory • Provided by the NASA Astrophysics Data System

1985A&A...146...38K

Table 2. Red radio galaxies with spectroscopic redshifts (in order of F)

Name	Type	z	F	J-F	$S_{1.4}$ (mJy)	LAS (")	α_{21}^{50}	M_F	$\log P_{1.4}$ (W/Hz)
54W009	G GR	0.083	15.71	1.25	5.99	22.5	-	-22.87	23.30
55W041	G	0.080	15.77	1.25	2.02	<8.6	0.12	-22.72	22.77
55W149	G GR	0.150	16.52	1.44	6.98	8.5	0.84	-23.45	23.90
53W020	G GR	0.100	17.03	1.29	6.74	7.3	1.07	-21.98	23.53
55W037	G	0.210	17.32	1.49	1520	114	0.76	-23.50	26.55
52W013	G CL	0.241	17.32	1.58	2.88	<17	0.51	-23.87	23.93
54W028	G	0.173	17.71	1.28	53.30	15.3	-	-22.61	24.91
52W044	G	0.300	18.75	1.71	10.20	25.1	0.67	-23.06	24.70
53W044	G	0.311	18.90	1.77	1.75	<8.5	0.92	-23.02	24.00
53W039	G CL	0.402	19.23	2.07	3.43	<11	0.82	-23.51	24.53
53W076	G	0.390	19.45	2.30	1.42	<9.4	<0.89	-23.19	24.13
54W017	G CL	0.512	20.24	2.08	10.76	23.8	-	-23.37	25.26
53W046	G	0.545	20.27	1.90	63.10	2.1	0.69	-23.58	26.08
53W079	G	0.548	20.76	1.83	13.25	8.4	0.05	-23.11	25.28
53W031	G	0.628	21.03	1.98	116.5	6.1	0.70	-23.39	26.49

bright spirals, and their radio powers ($22 \lesssim \log P_{1.4} \lesssim 22.7$) and spectral indices ($0.25 \lesssim \alpha \lesssim 0.50$) are consistent with their identification being a collection of H II regions or perhaps supernova remnants as in M 31 (see e.g. van der Kruit and Allen, 1976). In these galaxies the dominant radio emission is clearly extranuclear. These galaxies are not listed in Table 3.

For all other spiral galaxies the radio sources coincided with the galaxy nucleus. Without exception, these radio sources were unresolved with the 12″ beam at 21 cm. Although this is partially because fainter radio sources are harder to resolve, the upper limits to their angular sizes (in general <5–$15''$) are consistent with the radio sources being quite small (generally <5–35 kpc).

3.3. Faint radio galaxies ($18 < F < 21.5$)

The magnitude range $18 \lesssim F \lesssim 21.5$ is ideal for this survey. The magnitudes and colors are expected to be accurate; the separation of stellar images from extended images is not ambiguous; and, at least among the brighter objects, complex structure such as the presence of a thin disk or close companions can be seen. Effects due to cosmological evolution are in principle observable at this depth. The giant ellipticals associated with powerful radio sources attain redshifts greater than 0.5 by $F \sim 21$, corresponding to a look-back time of one-third of the age of the Universe.

For these fainter radio galaxies, we first concentrate on the $J-F$ vs. F color-magnitude diagram (Fig. 3a). The predicted $J-F$ vs. F relation for the nonevolving and mildly evolving giant elliptical models of Bruzual (1983) are indicated. The latter ($\mu=0.7$) model has a star formation rate exponentially declining with time, such that 70% of the galaxy mass is processed into stars during the first Gyr after formation. (Bruzual's evolving C-model, which has constant star-formation during the first Gyr and no star-formation afterwards, is intermediate between the nonevolving and the $\mu=0.7$ model and is not plotted in Figs. 3–6.)

3.3.1. Faint red galaxies

It is evident from Fig. 3a that our photometric depth and quality has revealed a large number of faint red ($J-F \sim 1.4$–2.4) galaxies. These may be identified with "classical" giant elliptical radio galaxies: they have high optical luminosities as we shall substantiate below, but to avoid undue prejudice, we shall usually refer to this class of radio source as R radio galaxies. The R galaxies dominate the interval $18 < F < 21.5$, beyond which the J data become incomplete (oblique dotted line in Fig. 3a). The important point is that our data show no evidence for the *lack* of faint red radio galaxies. This is confirmed in the $F-N$ vs. F color-magnitude diagram (Fig. 3c), where the population of red radio galaxies exists at least to $F \sim 22.0$. Beyond this, there do exist several objects that are very red in $F-N$, although these are so faint that their classification may be in error.

The luminosity of these faint radio galaxies can only be reliable *determined* from redshifts derived from slit spectroscopy, although broadband colors (if the intrinsic spectra are assumed) and magnitudes (if the luminosities are assumed) can be used to *estimate* redshifts. The fair fit in Fig. 3a of the color-magnitude relation predicted for luminous giant ellipticals to the colors observed for our red radio galaxies suggests that these radio galaxies as a class are likely to be luminous. Fortunately, we have enough reliable redshifts for R radio galaxies to address the question directly. The redshift data are shown in Fig. 5 (F vs. z) and Fig. 6 ($J-F$ vs. z).

© European Southern Observatory • Provided by the NASA Astrophysics Data System

1985A&A...146...38K

Table 3. Blue radio galaxies with spectroscopic redshifts (in order of F)

Name	Type	z	F	J-F	$S_{1.4}$ (mJy)	RES	α_{21}^{50}	M_F	$\log P_{1.4}$ (W/Hz)
			$F < 16^m$ galaxies						
54W008	spiral	0.015	14.0	0.75	12.08	U	-	-20.8	22.09
55W020	spiral	0.040	14.72	0.96	2.37	U	1.10	-22.25	22.25
53W072	spiral	0.019	15.09	1.17	6.56	U	0.17	-20.23	22.03
52W037	v.high SB	0.023	15.14	0.44	4.77	U	0.79	-20.60	22.06
55W178	spiral	0.041	15.49	0.92	1.24	U	1.41	-21.53	22.00
53W058	spiral w/ hot spot	0.034	15.61	1.13	1.39	U	<0.52	-21.00	21.87
			$16^m < F < 21^m$ galaxies						
53W003*	interact. double	0.050	16.09	0.86	3.19	U	0.38	-21.38	22.57
55W135	interact. mess	0.089	16.25	0.86	2.38	U	0.68	-22.54	22.96
54W032*	v.high SB	0.097	16.24	0.31	8.75	U	-	-22.75	23.60
52W020	SO/a	0.060	16.53	1.06	3.06	U	1.08	-21.35	22.72
53W090	compact	0.094	16.90	0.67	2.06	U	<0.83	-22.01	22.95
54W018	barred Sp	0.038	17.08	0.82	3.22	U	-	-19.77	22.33
52W036*	peculiar	0.240	17.38	0.99	1.03	U	1.20	-23.81	23.55
55W077	double	0.126	17.47	1.11	8.75	U	0.59	-22.13	23.83
55W137	interact. mess	0.160	17.8	0.9	1.60	U	1.72	-22.38	23.38
54W013	pec (jet?) compact	0.249	17.99	0.58	1.51	U	-	-23.29	23.70
52W023	v. compact (merger?)	0.202	19.65	0.40	1.22	U	1.47	-21.10	23.47
54W053	double	0.302	20.63	0.69	2.82	U	-	-21.16	24.16
53W071	elongated	0.287	20.90	1.08	2.78	U	1.44	-20.75	24.18
52W012	in cluster	0.400	22.11	0.99	10.02	U	1.14	-20.44	25.04

(*) Not in complete radio sample, but bona fide identification.

The spectroscopic redshifts of the faint R radio galaxies in Fig. 5 and Table 2 confirm the claim that they are luminous and can be considered as "standard candles". For $F > 18$, the R galaxies have radio powers of $\langle \log P_{1.4} \rangle = 25.1 \pm 0.9$, and optical luminosities of $\langle M_F \rangle = -23.3 \pm 0.2$. Auriemma et al. (1977) and Meier et al. (1979) have suggested that radio galaxies with radio powers just below the break observed locally in the RLF (at $\log P^* \sim 25.0\, WHz^{-1}$) can be optically underluminous compared with the more powerful sources. For the five giant ellipticals in our sample with $\log P_{1.4} > 25$, we observe $\langle M_F \rangle = -23.4 \pm 0.2$ (s.d.), while for the ten giant elliptical with $\log P_{1.4} < 25$, we find $\langle M_F \rangle = -23.0 \pm 0.5$. The optical luminosities of all 15 giant ellipticals are mostly in the range $-23.5 \lesssim M_F \lesssim -22.0$ with $\langle M_F \rangle \simeq -23.2 \pm 0.5$. We cannot, of course, exclude the possibility that some of the radio galaxies for which we have no spectroscopic data are less luminous. However, those R radio galaxies for which we do have redshifts should be typical of all radio galaxies of this type. This is confirmed by their distribution in the $J-F$ vs. F color-magnitude diagram, which is similar to those of the other red galaxies without measured spectra.

Figure 6 shows that the R radio galaxies have intrinsic continuum spectra like those of giant elliptical galaxies. A similar color-redshift relation was found for the 3CR giant ellipticals by Kristian et al. (1978). If the R radio galaxies at $F \sim 21$ are standard candles, then their redshifts are near 0.6 (Fig. 5). Thus, *at least some* radio galaxies at that redshift do *not* manifest strong optical color or luminosity evolution.

According to Figs. 3a, 5, and 6, the evolving models appear to describe the R radio galaxies somewhat better than does the unevolving model, although the difference is slight. Note that Fig. 3a shows that the R galaxies are also somewhat bluer than the model at *bright* magnitudes, which is more reasonable interpreted as a systematic problem with the model energy distribution, or with the color zero point, or both. Whatever the problem is at

© European Southern Observatory • Provided by the NASA Astrophysics Data System

1985A&A...146...38K

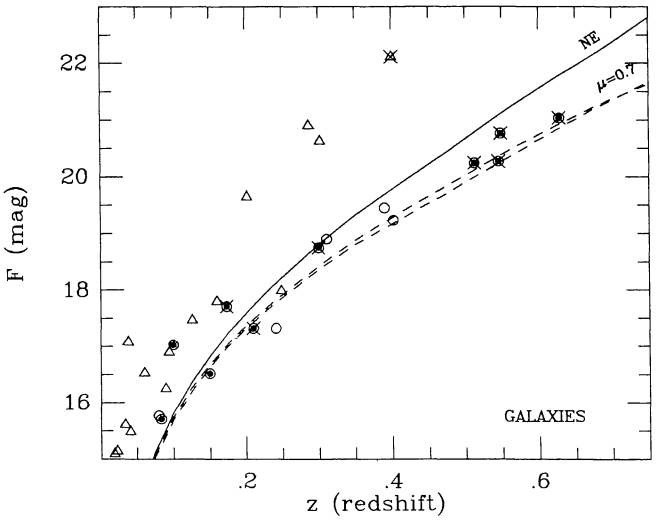

Fig. 5. F magnitude vs. redshift for all radio galaxies in the complete optical-radio sample with reliable redshifts. For symbols and models, see Fig. 3a

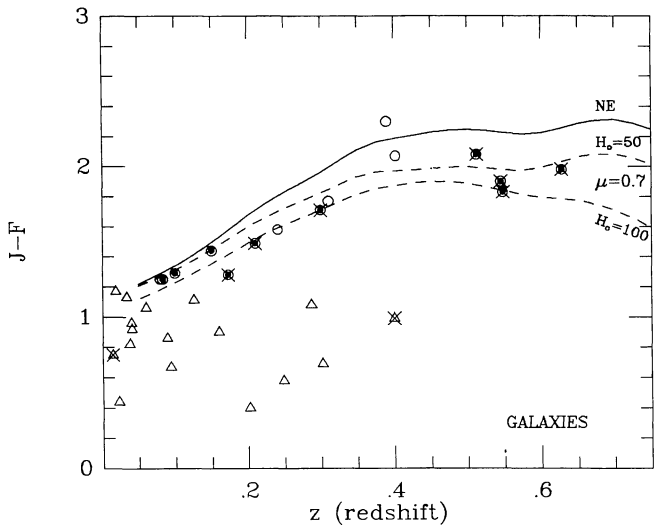

Fig. 6. $J-F$ color vs. redshift for all radio galaxies in the complete radio-optical sample with reliable redshifts. For symbols and models, see Fig. 3a

bright magnitudes, there is no reason to believe that it vanishes at fainter magnitudes The $F-N$ vs. N color-magnitude diagram (Fig. 3c) is consistent with little or no color evolution for the red radio galaxies, although the distinction between the nonevolving and evolving ($\mu=0.7$) model predictions for giant ellipticals is smaller than in Fig. 3a.

In conclusion, Fig. 5 shows that the F magnitudes for the high redshift R radio galaxies are indeed somewhat brighter than the no-evolution $q_0=0$ line, and Fig. 6 shows that their colors are somewhat bluer, as is the case for some of the 3CR radio galaxies of Kristian et al. (1978). However, the differences between the data and the no-evolution (or passive-evolution) model are not sufficiently large to make claims for the detection of *strong* optical evolution. We have shown, in any case, that there are wihin the observational uncertainties at least some high-redshift radio galaxies that are much like radio galaxies at $z=0$.

Two other possible causes of bluer colors should be considered. At higher redshifts, the photographic J band samples the rest frame ultraviolet. Since nearby giant ellipticals have been found to have a wide range of UV/blue colors (e.g. Bertola et al., 1982), a larger dispersion in the measured $J-F$ colors of high-redshift giant ellipticals which are bluer than present-day ellipticals would not prove that *all* of them, radio sources or not, have undergone color evolution. Furthermore, it is possible that the presence of a radio source is at least weakly correlated with a hotter-than-average UV spectrum, an effect suggested by the data of Kristian et al. (1978) for some of the powerful 3CR radio galaxies. The rather small dispersion in color for our red galaxies in the color-redshift diagram suggests that these effects are probably not large.

3.3.2. Faint blue galaxies

We consider now the nature of the blue radio galaxies in the interval $18 \lesssim F \lesssim 21.5$ which we called B radio galaxies. We have a small but useful number of redshifts for these (Figs. 5 and 6). None of the redshifts is greater than 0.4. These galaxies are an unusual class of radio source. Table 3 summarizes data from Table 1 for B radio galaxies with reliable redshifts. Their radio powers are in the range $22.5 < \log P_{1.4} \lesssim 24.2$ with $\langle \log P_{1.4} \rangle \sim 23.5 \pm 0.7$. This average radio power is higher than that of ordinary spirals, being actually closer to that of Seyfert and Markarian galaxies (Meurs, 1982), but is still below the break of the radio luminosity function of the elliptical galaxies (Auriemma et al., 1977). The optical luminosities of the blue radio galaxies are generally in the range $-23 \lesssim M_F \lesssim -20$, with $\langle M_F \rangle \sim 21.8 \pm 1.1$, very similar to M^* for field galaxies. Since the spiral radio galaxies with $F < 18$ were also close to M^*, the average radio-to-optical flux ratio of the fainter blue galaxy class is higher by about a factor 10.

Unfortunately, we have few redshifts for the blue galaxies fainter than $F=20$. At least a rough idea of the redshifts can be obtained in principle from the colors (Koo, 1981), but the bluest galaxies are the most difficult cases in this respect. Figure 4 gives a $U-J$ vs. $J-F$ plot for all galaxies in the interval $21 \leqq J \leqq 22$ that can be directly compared to the *field* color distribution published by Koo and Kron (1982) as their Fig. 4. Our Fig. 4 shows that: (a) the B and R classes are well-separated in the color-color diagram; (b) the proportion of R to B galaxies if *far* higher than for a random field population; and (c) the redshifts are not especially high – the model in fact overestimates the redshifts for two of the four radio galaxies with known redshifts.

For $F < 21.5$ there were only four blue radio galaxies with $S_{1.4} > 9$ mJy among which only two were resolved radio sources at 21 cm (Fig. 3a). Thus, with these few exceptions, galaxies with $F < 21.5$ that have $S_{1.4} > 9$ mJy or that are resolved at 21 cm, are *all* associated with luminous giant ellipticals. Because most blue galaxies have fluxes below 10 mJy, usually only an upper limit to their angular size could be found in Paper I, which is of the order 10″–15″. Their radio spectral indices span a wide range, $-1.0 \lesssim \alpha \lesssim +1.75$ (see Fig. 7a), larger than the error distribution in α can reasonably explain. The dispersion in spectral index of the blue radio galaxies may be partially intrinsic, possibly caused by nuclear variability.

A clue to the nature of the faint blue galaxies is revealed by their peculiar optical morphologies, often suggestive of interacting pairs or mergers. Table 3 shows that the proportion of galaxies with peculiar optical morphology is higher for the fainter B radio galaxies. Perhaps these radio galaxies are, in some sense, analogous to Perseus A, Centaurus A, and Fornax A. Roos (1981, 1985) has discussed a physical mechanism in which interacting or merging galaxies may have enhanced nuclear activity. For a sample of 18 optically selected merger candidates, Heckman (1983)

© European Southern Observatory • Provided by the NASA Astrophysics Data System

1985A&A...146...38K

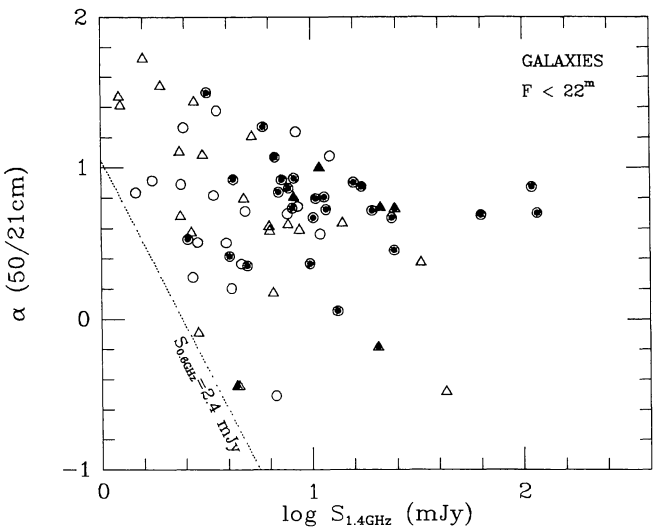

Fig. 7a. Spectral index α_{21}^{50} vs. flux density $S_{1.4}$ for all radio galaxies (except for 55W037, which has $S_{1.4}=1520$ mJy, $\alpha=0.76$) in the optical-radio complete sample with $F<22$. For symbols, see Fig. 3a. The completeness limits are about $S_{0.6}=2.4$ mJy (dotted) and $S_{1.4}=1.0$ mJy (left boundary)

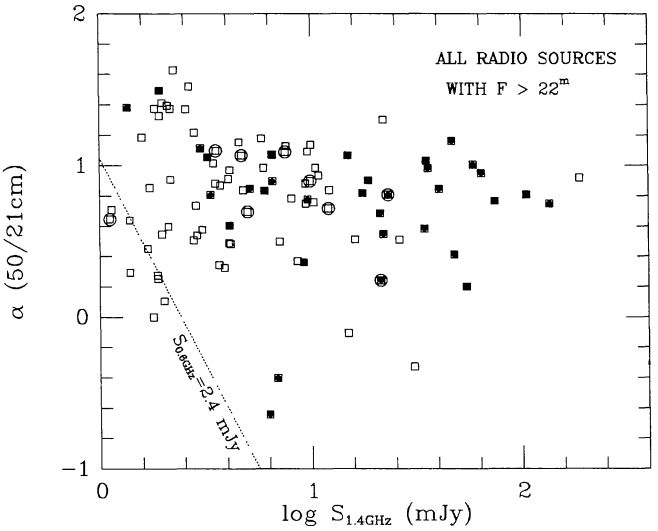

Fig. 7c. Spectral index α_{21}^{50} vs. flux density $S_{1.4}$ for all objects in the *radio*-complete sample with $F\geqq 22$. All objects are plotted as open squares, while red objects ($F-N>1.4$) are marked by a larger circle embracing the square. Resolved sources are indicated by interior-filled circles

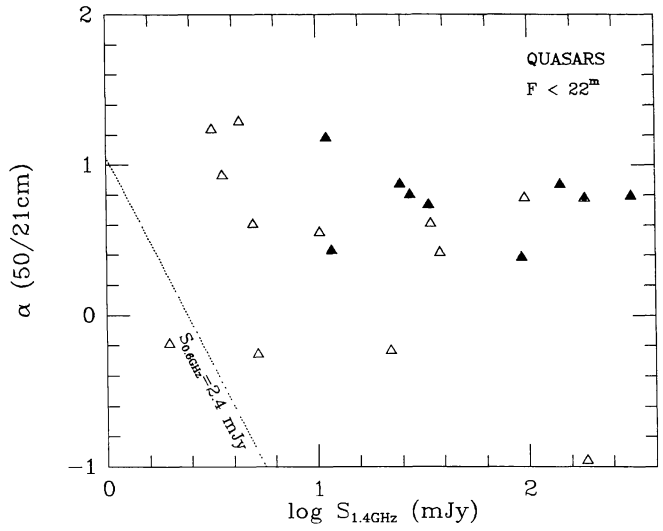

Fig. 7b. Spectral index α_{21}^{50} vs. flux density $S_{1.4}$ for quasars in the optical-radio complete sample with $F<22$. The symbols have the same meaning as those in Fig. 3b

also found that the radio luminosities are considerably higher ($\langle \log P_{1.4}\rangle \sim 23.0\pm 0.5$) than those of normal spiral galaxies of comparable optical luminosity. The radio luminosity of these mergers are very similar to the values found for our blue radio galaxies, although Heckman's optical luminosities ($\langle M_B\rangle \sim -22.1 \pm 0.8$) are somewhat higher than ours.

3.3.3. Summary of the red and blue radio galaxies for $F<21.5$

The picture we have developed so far can be summarized as follows:

For $S_{1.4}\gtrsim 9$ mJy, virtually all radio galaxies belong to the class of apparently red galaxies, which in optical respects, is like the much more powerful 3CR giant ellipticals. Essentially all identified *resolved* radio sources are associated with these red galaxies, consistent with the well-known fact that the large, extended extragalactic radio sources identified with galaxies are almost exclusively giant ellipticals. These radio galaxies form a remarkably homogeneous class, and display, at most, only weak evidence for optical evolution. The redshift depth to which we are sensitive is not sufficiently high to reverse the trend of redder colors with increasing redshift, so that all intrinsically red galaxies are seen as apparently red.

Below $S_{1.4}\lesssim 9$ mJy, there is another class of radio galaxy that is bluer (Fig. 3a). The brighter members look like ordinary disk systems (almost all late-type spirals), but the fainter members frequently have peculiar optical morphology. For example, there are cases of high compactness (52W023, 54W013), high surface brightness (52W037, 54W032), and several examples of doubles or mergers (54W053, 55W077, 55W135). The fainter B radio galaxies have higher radio/optical flux ratio when compared to the normal spiral galaxies. Thus, the B category may consist of more than one physical class, but on the other hand, the bright and faint B galaxies have some things in common: both groups have some representatives with steep radio spectra and most of them are unresolved radio sources at the 12″ beam. Also, the optical luminosities of the bright spirals and the fainter blue radio galaxies are similar. More spectroscopic work is required for a better understanding of these faint blue galaxies. In any event, we have every reason to believe that there is a clear distinction between the B and the R category.

The existence of a sizeable population of faint blue radio galaxies was also noted by Katgert et al. (1979), who proposed a picture different from the one we have sketched above. Their data consisted of heterogeneous, eye-estimated magnitudes and colors, and the star/galaxy image separation was generally done from 48″ Schmidt plates. In the absence of spectroscopic redshifts, they assumed that the faint blue radio galaxies were actually generically related to the brighter red radio galaxies, and suggested that the former were luminous ellipticals at high redshift seen during an early blue phase. This line of thought was later also expressed by Windhorst et al. (1982) and van der Laan and Windhorst (1982). The color-magnitude diagrams, upon which that argument was

© European Southern Observatory • Provided by the NASA Astrophysics Data System

1985A&A...146...38K

based, looks quite different from our Fig. 3a. The data presented here are properly calibrated, more accurate, more homogeneous, and less affected by misclassified quasars. Also important for the interpretation, is the greater certainty in the optical completeness limits in the present study. Finally, and most importantly, the current study incorporates spectroscopic information as well. It is therefore not surprising that we reach a different conclusion.

3.4. *Very faint objects* ($F>21.5$)

The optical data for the $F \geqq 21.5$ objects are characterized by less certain star/galaxy image classification, only one reliable galaxy redshift, larger $J-F$ color errors, greater incompleteness, and proportionally more blue objects (Fig. 3a).

3.4.1. Very faint red objects

The apparently larger number of faint blue objects for $F>21.5$ is at least partially illusory: due to incompleteness in the J band setting in around $J=23.5$ to 23.7, galaxies with $J-F>2$ would be unmeasurable in J. In Fig. 3c, several objects have $F>21.5$ and $F-N>1$, and are indeed unmeasurable in J (these objects are listed in Table 4). Thus, their $J-F$ colors are likely to exceed 2.0. Placing these extra red galaxies in the upper-righthand region of Fig. 3a would change the apparent distribution quite drastically. In fact, the majority of the radio galaxies fainter than $F=21$ could well be red.

The radio properties of the one dozen $F>21.5$ radio galaxies that are unmeasurably faint in the J band are as follows (Table 4). All have flux densities smaller than 10 mJy (see also Fig. 7c). Most have rather steep radio spectra ($0.8 \lesssim \alpha \lesssim 1.2$). Thus, it is possible that the red galaxies with $F>21.5$ are indeed the counterparts of the red galaxies at $F<21.5$, whose properties are known to be like "standard-candle" giant elliptical radio galaxies. The implied redshift for the $F>21.5$ red radio galaxies is ~ 0.8. Their radio sources are, however, unresolved (with one exception), but this could be a distance effect, possibly in combination with smaller intrinsic sizes at earlier epochs.

We conclude that down to the detection limit of the red 4 m plates, there exists a population of red galaxies likely to be at high redshifts and unlikely to all have experienced dramatic color evolution. (If the very faint red objects were instead lower luminosity ellipticals, they could be quite red even for redshifts not larger than $z \sim 0.3$. But, the existence of even a small number of red giant ellipticals at high redshift would call into question any claim that color evolution has occurred universally, at least, if we assume all galaxies were formed at the same time.)

Table 4. Red objects detected in F and N but not in J

Name	Type		F	F-N	$S_{1.4}$ (mJy)	RES.	α_{21}^{50}
52W039	?		22.98	2.13	3.56	U	1.10
53W005	G	GR	22.82	1.84	7.58	U	1.09
53W021	Q?	GR	22.32	1.56	4.71	U	1.07
54W014	?		22.03	1.29	5.47	U	-
54W039	G		21.85	1.78	8.39	R	-
55W007	G	CL	21.41	1.67	8.47	U	1.24
55W046	G		22.77	2.41	9.91	U	0.90
55W065	G?		21.79	2.61	2.72	U	0.28
55W093	G?		21.63	1.28	1.46	U	0.84
55W116	G		21.81	1.20	0.96	U	<1.25
55W160	?		22.08	1.37	0.85	U	0.76
55W166	G		21.96	1.85	2.40	U	0.89

3.4.2. Very faint blue objects

We consider now those objects with $F>21.5$ and $J-F \lesssim 1.6$. Three obvious possibilities, alone or in combination, for the nature of these blue galaxies are:

(1) the direct or possibly (at radio wavelengths) evolving counterparts of the brighter blue galaxies; (2) the UV bright, but otherwise normal, giant ellipticals, which appear blue due to the UV entering our passbands (say $z \sim 0.6$ to $z \sim 1.0$); and (3) the intrinsically blue and very luminous evolving giant ellipticals seen at high redshift ($z>1$) during an epoch of high star-formation rate.

Unlike the situation for $F<21.5$, several of the faint blue objects are associated with radio sources stronger than $S_{1.4}=9$ mJy, and are *resolved* with the 12″ beam. Thus, taken at face-value, the faint blue radio galaxies with resolved radio morphologies or $S_{1.4}>9$ mJy, or both, could support an argument for the existence of *some* giant ellipticals seen in a bright, early phase. However, two such objects, 53W026 and 55W066, could be blue, mainly due to photometric error: both galaxies are in the domain of elliptical galaxies in the $F-N$ vs. F diagram (Fig. 3c). Furthermore, some contamination of the galaxy sample by quasars will occur for $F>21.5$. Finally, the few expected misidentifications (14 out of 171 objects, see Paper II) are probably associated with random field galaxies, which are faint and relatively blue. Together with photometric errors, these two effects account for at least some fraction of the faint blue galaxies and possibly *all* of the *unusual* blue galaxies which have $S_{1.4}>9$ mJy or are resolved radio sources. We thus find no compelling evidence to support either the unevolving UV-bright hypothesis or the evolving gE hypothesis for $F>21.5$. The lack of supporting evidence from our photometry does *not* imply that these hypotheses are wrong; only solid redshifts can supply conclusive constraints upon the nature of the faint blue radio galaxies.

3.4.3. Unidentified radio sources

Figure 7c shows the radio flux densities and spectral indices of the optically *unidentified* or otherwise $F>22$ sources (plate-limit objects). Their spectral index distribution may be somewhat displaced towards steeper spectra ($\alpha_{med} \sim 0.85$). For the identified galaxies the median spectral index is about $\alpha_{med} \sim 0.70$. This effect is in agreement with the result of Tielens et al. (1979), who found a significantly smaller identification fraction for steep spectrum radio sources than for flat spectrum sources down to the Palomar Sky Survey limit, albeit at the 3CR and 4C level. In our mJy sample, the effect is not as strong as at the Jy level. Blumenthal and Miley (1979) offered an interpretation whereby steep spectrum radio sources may be distributed towards higher redshifts when compared to flat spectrum sources, a result modeled in more detail by Peacock and Gull (1981).

© European Southern Observatory • Provided by the NASA Astrophysics Data System

1985A&A...146...38K

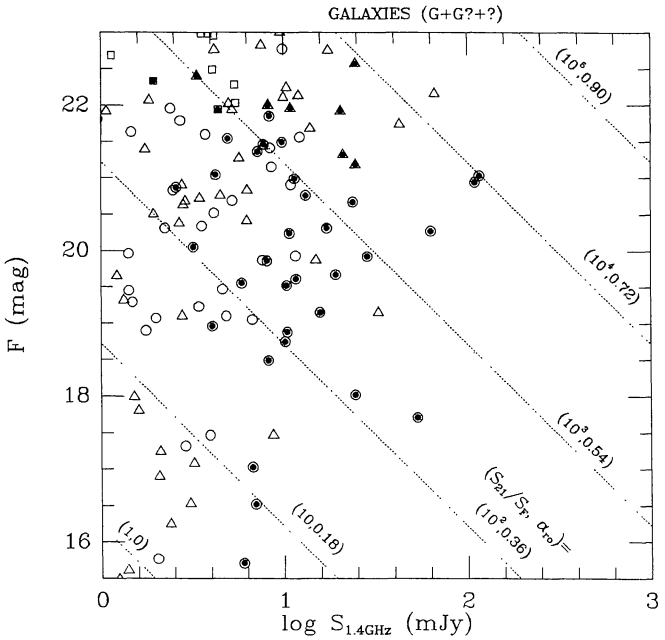

Fig. 8a. F magnitude vs. flux density $S_{1.4}$ for all radio galaxies in the radio-optical complete sample. The symbols are defined in the caption to Fig. 3a. Lines of constant radio-to-optical spectral index denote monochromatic radio-optical flux ratios $S(21\,\mathrm{cm})/S(6100\,\text{Å})=1, 10, 10^2, 10^3, 10^4$, and 10^5 with corresponding radio-optical spectral index $\alpha_{ro}=0$, 0.18, 0.36, 0.54, 0.72, and 0.90

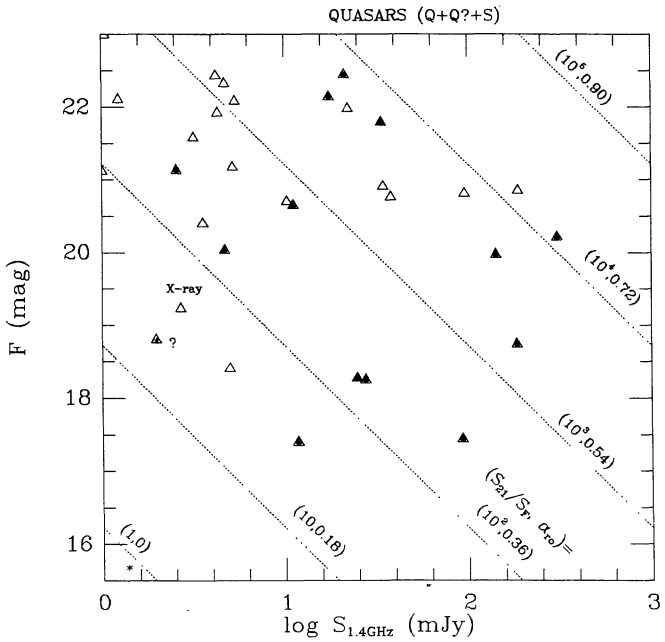

Fig. 8b. F magnitude vs. flux density $S_{1.4}$ for all quasars in the radio-optical complete sample. Symbols are as for Fig. 3b, except that the Galactic star 55W127 (and a possible one, 55W163) are marked by an * (and by *?). The X-ray quasar is also indicated. The lines are as in Fig. 8a

In Fig. 7a, most identified radio sources with $S_{1.4}>9$ mJy are resolved with the 12″ beam and were identified as R galaxies. Figure 7c shows that most of the unidentified radio sources with $S_{1.4}>9$ mJy are also resolved at 21 cm. Thus, in concordance with conclusions from Figs. 7a and 3a, the unidentified resolved radio sources with $S_{1.4}>9$ mJy could be mostly of the same R galaxy class. On the other hand, a substantial contribution by optically finat quasars cannot be easily ruled out since these have a similar α_{21}^{50} vs. $\log S_{1.4}$ distribution (Fig. 7b). As shown in Fig. 8b, quasars are relatively rare when compared with galaxies for $S_{1.4}>9$ mJy and $18<F<21.5$. Thus, unless there is a dramatic change in the ratio of quasras to galaxies, we expect the unidentified radio sources to be mainly associated with galaxies. Below 9 mJy, the proportion of B galaxies is likely to be greater.

4. Stellar objects

4.1. *Quasars*

Among a total of 24 identified radio sources brighter than $F=18$, there are two quasars: 53W009 is a quasar with $z=1.09$ and 53W022 is a blue stellar object. The fainter stellar objects are probably all quasars with the possible exception of 55W163 (see Sect. 4.2).

The relatively small number (20) of stellar identifications in the range $18\lesssim F\lesssim 21.5$, with only six having spectroscopic data, precludes at this time an extensive statistical study of radio-weak quasars (see e.g. Mitchell, 1983). The median flux of the stellar objects is about 9 mJy (Figs. 7b and 8b), most are unresolved at 21 cm, and their spectral index distribution (Fig. 7b) is not very different from that of radio galaxies (Fig. 7a). Both the radio galaxies and the quasars have a median spectral index close to 0.70.

The quasar, 53W080, at $z=0.546$ is noteworthy because it appears to be in a cluster, and its redshift is virtually identical to that of two other radio galaxies in its vicinity, 53W046 and 53W079. The angular scale is 0°.6 corresponding to a linear scale of 16 Mpc. All three radio source identifications are probably in the same supercluster at $z\sim 0.55$.

Most of the radio-selected quasars have colors typical of optically selected samples (Koo and Kron, 1982). The clear exceptions (all in Hercules and Lynx) appear red in $U-J$ or $J-F$ (e.g., 53W075 with $J-F=1.3$; see Fig. 3b), but since the UJF plates in Hercules and Lynx were obtained at different epochs (Table 1 of Paper II), these objects may be variable and may not be red intrinsically.

4.2. *Radio stars*

Among the few bright stellar objects, 55W127 is a spectroscopically confirmed star of intermediate type. The identification with a bright star is unusual but not unreasonable, given the good radio-optical positional coincidence in this case, and the very low radio-to-optical flux ratio ($S_{1.4}=1.3$ mJy, $F=15.6\simeq 1.8$ mJy, $\alpha_{ro}\simeq -0.03$; see also Fig. 8a and b, to be discussed in Sect. 5). The star itself is found to be variable at 21 cm (Oort and Windhorst, 1985). Moreover, its very steep radio spectral index ($\alpha_{21}^{50}\simeq 1.45$, Paper IV) is presumably the consequence of this variability. Another star candidate is 55W158 ($S_{1.4}\sim 0.7$ mJy), which is variable on a time scale of one year; the radio source identification is probably a faint galaxy close to the $F\sim 18$ star, although the star cannot be ruled out as the correct identification (Paper II). Since the radio-optical spectral index of the star ($S_F\sim 0.2$ mJy or $\alpha_{ro}\simeq +0.1$) is similar to the very flat radio-optical spectrum of 55W127, the star may, in fact, be the correct identification of 55W158. A third fainter radio star candidate is the red stellar object, 55W163. This radio source has $S_{1.4}\sim 2$ mJy, and is also variable at 21 cm (Oort and Windhorst, 1985), hence it could be a star similar to 55W127. It has a very flat spectral index ($\alpha_{21}^{50}\simeq 0.2$, Paper IV) and a flat radio-optical spectral index ($\alpha_{ro}\simeq +0.24$).

© European Southern Observatory • Provided by the NASA Astrophysics Data System

1985A&A...146...38K

With only a few star identifications down to ~ 1 mJy there is no reason to believe that very deep (sub-mJy) radio surveys will be dominated by radio stars, although as a class, they could be interesting objects (X-ray sources?).

5. The bivariate flux density distribution

In Sect. 3, we have shown that faint radio sources can be associated with two major populations, namely a luminous red class of giant elliptical radio galaxies (R), and a generally (intrinsically) fainter blue class of radio galaxies (B). No evidence for strong optical color evolution was found for the first class, nor for the existence of non-standard-candle R radio galaxies. The R radio galaxies can thus be used to determine the radio luminosity function directly, merely by counting the number of such galaxies in bins of radio flux density and magnitude. That is, the magnitudes serve as a measure of redshift as observed in Fig. 5. Possible effects of optical luminosity evolution on these surface densities are eliminated by adopting the experimentally defined, monotonic and one-to-one relationship between magnitude and redshift to $z=0.6$.

A schematic representation of the observed bivariate (radio-optical) flux density distribution is given by the distribution of points in the F-magnitude vs. $\log S_{1.4}$ plane for radio galaxies (Fig. 8a) and for quasars (Fig. 8b). Qualitatively, the density of points increases strongly towards fainter magnitudes and fluxes. Quantitatively, this is substantiated after accounting for the weights. In Fig. 8, lines of constant monochromatic radio-to-optical flux ratio are drawn for $S_{1.4}/S_F = 1$, 10, 10^2, 10^3, 10^4, and 10^5, labeled with the corresponding radio-optical spectral index and assuming for simplicity no K-correction. Radio selected quasars have, in general, higher radio-to-optical flux ratios than galaxies. Most quasars are in the range $0.25 \lesssim \alpha_{ro} \lesssim 0.75$, while the radio star, 55W127, and the possible stars, 55W158 and 55W163 have $\alpha_{ro} \lesssim 0.25$. Our only X-ray detected quasar, 54W073, has $\alpha_{ro} \sim 0.30$ and $\alpha_{ox} \sim 1.1$. For comparison, at the 3CR and Parkes level Zamorani et al. (1981) found that most of their quasars have $0.4 \lesssim \alpha_{ro} \lesssim 0.9$ and $1.0 \lesssim \alpha_{ox} \lesssim 1.7$.

Since a detailed analysis of the evolution of the radio luminosity function will be made in a later paper (Windhorst et al., 1984), here we give only a brief discussion. We have binned the class R radio galaxies by radio flux density and F magnitude in Table 5, where the surface densities (numbers/degree^2) are obtained by adding the individual radio source weights (listed in Table 1) and dividing by our total survey area of 5.52 deg^2. For comparison, Table 5 incorporated a no-evolution prediction of giant ellipticals that was computed following Katgert et al. (1979), who used the Auriemma et al. (1977) bivariate radio-optical luminosity function. Because the radio spectral index is, in general, close to unity, the radio K-correction is negligible. In this calculation, we assumed a standard candle with $M_F = -23.3$ ($H_0 = 50\,\mathrm{km\,s^{-1}\,Mpc^{-1}}$ and $q_0 = 0$) and Bruzual's (1983) K-correction.

Despite the small statistics, Table 5 shows that the observed surface densities of R galaxies are consistent with the prediction for $F \lesssim 18.5$, corresponding to $z \leqq 0.25$. Thus, no evolution in the radio luminosity function is implied out to this distance, consistent with the findings of Katgert et al. (1979) and of Robertson (1980). In

Table 5. The bivariate (radio-optical) flux density table for red galaxies

F =	14.5	16.5	17.5	18.5	19.5	20.5	21.5	22.5
log $S_{1.4}$/mJy								
0.1								
	(1)	(1)	(0)	(4)	(2)	(3)	(3)	
	1.01	0.36	0.00	4.22	1.28	2.06	1.44	
	0.16	0.24	1.62	2.67	2.27	1.87	1.58	
0.5								
	(1)	(3)	(0)	(5)	(4)	(6)	(2)	
	0.28	0.63	0.00	1.50	1.32	1.44	0.57	
	0.11	0.69	1.07	0.97	0.82	0.68	0.57	
0.9								
	(0)	(1)	(1)	(3)	(7)	(6)	(2)	
	0.00	0.18	0.21	0.62	1.43	1.11	0.37	
	0.26	0.38	0.39	0.35	0.30	0.25	0.21	
1.3								
	(0)	(0)	(1)	(0)	(1)	(2)	(0)	
	0.00	0.00	0.18	0.00	0.18	0.36	0.00	
	0.20	0.14	0.14	0.13	0.11	0.09	0.08	
1.7								
	(0)	(0)	(1)	(0)	(1)	(2)	(0)	
	0.00	0.00	0.20	0.00	0.20	0.36	0.00	
	0.081	0.051	0.051	0.046	0.039	0.032	0.027	
2.1								

The number of red galaxies per bin is given between brackets. The second number in each bin is the observed surface density (deg^{-2}) accounting for the weights induced by the WSRT primary beam. The third number is the prediction for the unevolving E + S0 radio luminosity function of Auriemma et al. (1977). Calculations assume $M_F = -23.^m2$ and Bruzual's (1983) K-correction for an elliptical galaxy ($H_o = 50$ km s^{-1} Mpc^{-1} and $q_o = 0$).

© European Southern Observatory • Provided by the NASA Astrophysics Data System

1985A&A...146...38K

the text fainter magnitude intervals there is an excess of R radio galaxies over the prediction by about a factor of 2 to 5.

This effect is slightly stronger in the $20.5 < F < 21.5$ range, corresponding to $z \sim 0.7$, where the stronger radio sources are almost an order of magnitude more numerous, and the weaker radio sources show a smaller enhancement in number densities. For the faintest magnitude bin, the excess is not evident. However, this is probably due to the selection against red galaxies with $F > 21.5$ because of the J-plate limit (Fig. 3a).

6. Conclusions

We have combined the results of a deep ($S_{1.4} \gtrsim 1$ mJy) radio survey with multiband 4-m photographic photometry to $F \sim 22.7$, and a few dozen redshifts to give a reliable discussion of the nature of weak radio sources. We conclude:

(a) At bright magnitudes ($F \lesssim 18$), the radio source identifications are spiral galaxies, giant ellipticals with "standard candle" properties, and a few quasars.

(b) At fainter magnitudes ($18 < F < 21.5$) the population of weak radio sources consists of the "standard-candle" giant ellipticals, a class of blue radio galaxies which are often associated with close and possibly interacting neighbors, and some quasars.

(c) The giant elliptical galaxies are associated with extended radio sources with linear sizes in the range 20–200 kpc. The blue radio galaxies have smaller linear sizes (< 5–35 kpc).

(d) There is no evidence for strong optical color and luminosity evolution of giant elliptical radio galaxies out to redshifts of $z = 0.6$. For example, either the passively evolving C-model or the mildly evolving $\mu = 0.7$ model of Bruzual (1983) are consistent with the data. We found no convincing evidence for the existence of blue progenitor giant ellipticals in our sample. The very faint blue radio galaxies ($F > 21.5$) are probably the high redshift counterparts of the brighter blue galaxies.

(e) The evolution of the radio luminosity function was investigated by adopting the standard-candle hypothesis for the red (R) galaxies, as calibrated by our spectroscopy. The dependence of the number densities on redshift is described by an increasing density of the more powerful radio sources (at least beyond $z \sim 0.3$ and out to the optical limits of the present observations) and a slightly weaker evolution for objects of lower radio power.

We hope to clarify the nature of the optical luminosity function of both the R and B radio source classes with further spectroscopy. In particular, we intend to investigate whether or not the blue (B) radio galaxies have undergone evolution in either their optical spectra or their radio luminosity function.

Acknowledgements. This work was partially supported by NSF grants 79-20994 and 81-21653 of the United States. RAW acknowledges the Netherlands Organization for the Advancement of Pure Research (ZWO) for ASTRON/ZWO grant 19-23-009.

We gratefully acknowledge Kitt Peak National Observatory and McDonald Observatory for the generous allocation of telescope time. We thank Jim DeVeny for assistance with the Mayall Cryogenic Camera, Bill Schoening for help with the photographic process, and Paul Rybski and Dave Doss for help with the McDonald IDS. We acknowledge the use of the Midwest Astronomical Data Reduction and Analysis Facility (MADRAF) at Madison.

Both Harvey Butcher and Hy Spinrad measured several spectroscopic redshifts and allowed us to use them in advance of publication. Allan Sandage kindly made available his unpublished photoelectric sequence in SA28. Donald Hamilton and Andy Jankevics provide help with the spectroscopic data reduction and image processing software, of Marc Oort with the RLF model calculations and Gustavo Bruzual with his galaxy evolution models. RAW wishes to thank Harry van der Laan and Peter Katgert for stimulating discussions and their continuous support of the project.

The photographs were made by Richard Dreiser and Wim Brokaar and collated by Hedi Versteege. The manuscript was typed by Maria Anderson and Lijsbeth van der Poel.

Appendix

Several additional redshifts have been obtained since the text, figures, and tables were prepared. We therefore present these new redshifts, most of which were obtained at Kitt Peak in March 1984, in Table A1. The values given for M_F and $\log P_{1.4}$ for the R galaxies were computed as before, i.e., assuming Bruzual's K-corrections for evolving ellipticals, and $q_0 = 0$ and $H_0 = 50\,\mathrm{km\,s^{-1}\,Mpc^{-1}}$. For the B galaxies, the K-corrections are unknown, and we have adopted simply $K(F) \sim z$. No K-correction for the quasars was attempted, but in all cases, the radio spectral index was taken into account in the calculation of $\log P_{1.4}$.

Remarks on individual objects

The source, 55W163, is indeed a star, thus vindicating the discussion in Sect. 4.2. It is of intermediate type (consistent with its colors) with Mg and Na absorption, and is therefore like 55W127. These sources could be related to the radio stars discussed by Linsky and Gary (1983, *Astrophys. J.* **274**, 776), and deserve further attention.

The redshift for the quasar, 53W015, assumes that the single observed emission feature is Mg II, a likely identification considering the appearance of the line and its position within our spectral range. This feature is probably responsible for the relatively red $J-F$ color of the quasar, but the red color could also be due to variability, as discussed in the text. If the proposed redshift is correct, it is of interest to note the coincidence in redshift with 53W009 and with 3C356 ($z = 1.085$), which is $\lesssim 1$ degree away from the Hercules fields.

55W152 is not in the complete sample as defined in Paper II.

The B galaxy, 55W010, is unusual in almost every respect: it has very high optical luminosity and relatively high radio power. The radio source, 55W010, is clearly resolved into two components. The northern component is unresolved at the 12″ WSRT beam, and coincides with the B galaxy. The contour plot of Paper I shows that the overall radio morphology is very unusual, i.e., unlike a classical double or head-tail source. The southern component could be a superposed background source, as yet unidentified. The optical image of 55W010 is quite compact, yet the color is neutral, and the spectrum shows no emission lines. Its importance lies in the fact that it is one of the few relatively bright B galaxies with $S_{1.4} > 9$ mJy. Another example of a B galaxy with an unusually high optical luminosity is 54W013 (Table 3), but its radio power is considerably lower than that of 55W010. A nominal example of a B galaxy with high radio power, but which is much less luminous optically, is 52W012 (Table 3). However, in this case, further investigation suggests that the object for which the spectroscopy was obtained may not be the same as the object that

© European Southern Observatory • Provided by the NASA Astrophysics Data System

1985A&A...146...38K

Table A1

Name	z	F	$J-F$	$S^{1.4}$ (mJy)	RES	α_{21}^{50}	M_F	$\log P_{1.4}$ (W/Hz)
R galaxies								
55W105	0.196	17.47	1.26	3.9	*U*	0.51	−23.2	23.9
55W024	0.260	19.10	1.47	4.9	*U*	0.71	−22.3	24.2
55W044	0.265	19.15	1.52	15.8	*R*	0.90	−22.3	24.8
55W043	0.265	18.49	1.73	8.3	*R*	0.93	−23.0	24.5
55W043B	0.265							
55W056	0.295	19.05	1.82	6.7	*U*	−0.51	−22.7	24.4
53W045	0.30	19.29	1.88	1.5	*U*	<0.58	−22.5	23.8
55W063	0.30	18.02	1.88	24.5	*R*	0.46	−23.8	25.1
55W023	0.36	18.96	1.69	4.1	*R*	0.42	−23.4	24.4
53W032	0.37	18.88	1.57	10.5	*E*	0.80	−23.6	24.9
55W016	0.375	19.55	1.92	5.9	*R*	1.27	−22.9	24.8
53W076	0.39	19.45	2.30	1.4	*U*	<0.89	−23.2	24.1
B galaxies								
54W034	0.070	17.24	0.70	2.1	*U*		−21.0	22.7
55W152	0.115	(17.5)	(1.0)	2.2	*U*	0.72	−21.9	23.1
55W010	0.425	19.15	1.16	32.8	*U*	0.37	−23.7	25.5
Quasars								
55W179	0.465	18.41	0.65	5.0	*U*	0.61	−24.3	24.8
53W015	1.129	18.74	1.25	184.6	*R*	0.78	−26.4	27.3
Star								
55W163		18.80	1.15	2.0	*U*	−0.19	~ 5	12.9

was photometered, in view of inconsistencies in continuum shape and apparent brightness. In any case, 55W010 is unique.

Attention had been drawn to a galaxy about 12″ south of the nominal identification for 55W043, because of the compact morphology of the former – this object is listed as "55W043B" in Table A1. Its spectrum is characterized by a smooth continuum with strong emission, including lines of [Nev] and [Neiii], which, according to Spinrad (private communication), is very rare except in the most powerful radio galaxies. One is tempted to make the a posteriori claim that 55W043B is, in fact, the correct identification: indeed, precisely this line of argument was used to make the identification of 52W023 (Paper II). However, in the present case, the 21 cm and 50 cm positions agree to 2″, which would appear to rule out a positional error of the required size. 55W043B has not been photometered, but from Fig. 1, it can be seen to be considerably brighter and about the same color as 55W043, although from its spectrum, one would have expected its colors to be bluer. If 55W043 is the correct identification (as is assumed in Table A1), its properties are completely normal for its class. If 55W043B is the correct identification, it is overluminous, and even though its colors would put it in the R category, it is certainly not spectroscopically a gE galaxy.

There is evidently a redshift clump at $z=0.265$, consisting of 55W043, 55W043B, 55W044, and 55W024 (at $z=0.260$). 55W044 has companions both to the E and W (Fig. 1). The two galaxies to the E both have $z=0.265$, but the bluer and brighter galaxy to the W has $z=0.078$.

The galaxy 53W032 has strong forbidden emission lines, including [Neiii] (we did not detect Hβ in emission). This activity is very likely connected with the deviation of this galaxy from the normal color-redshift relation for gE galaxies.

55W063 is a classic example of a luminous first-ranked cluster galaxy.

General remarks

For a sample of eleven new R galaxy redshifts, $\langle M_F\rangle = -23.0\pm0.5$ and $\langle \log P_{1.4}\rangle = -24.5\pm0.4$. The sample is thus in no significant way distinguished from the sample already discussed in the text.

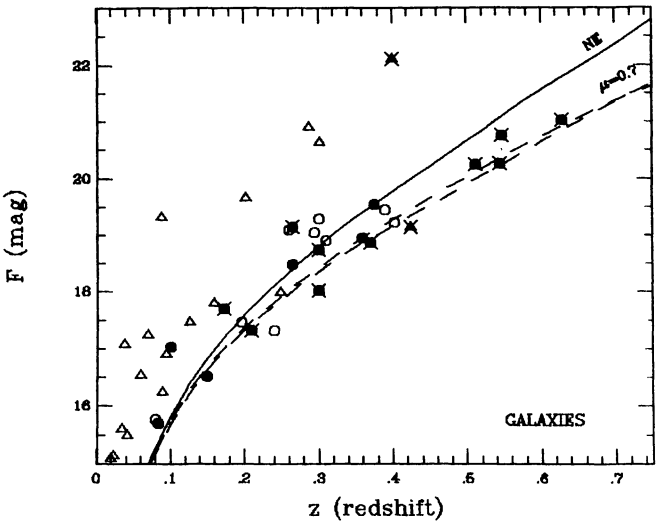

Fig. A5. F magnitude vs. redshift for all radio galaxies in the complete optical-radio sample, including the most recently obtained spectroscopic redshifts. For symbols and models, see Fig. 3a

© European Southern Observatory • Provided by the NASA Astrophysics Data System

1985A&A...146...38K

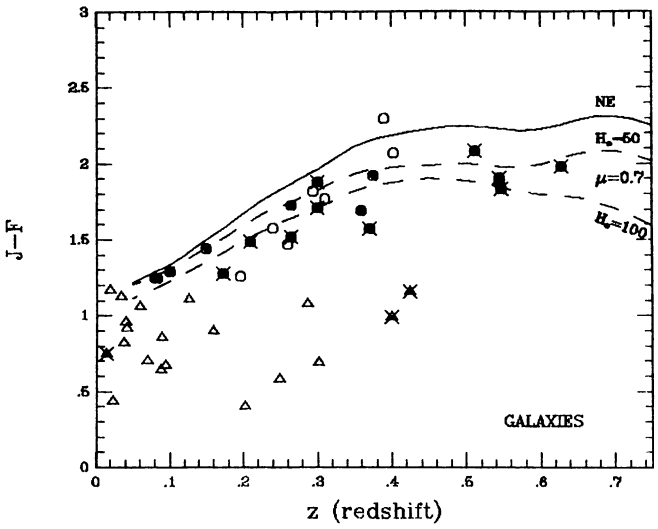

Fig. A6. $J-F$ color vs. redshift for all radio galaxies in the complete optical-radio sample, including the most recently obtained spectroscopic redshifts. For symbols and models, see Fig. 3a

There is, for instance, a good correlation seen in Table A1 between z and $J-F$ (with the exception of 53W032), which serves both to verify the quality of the photometry and to illustrate once again the essential homogeneity of the optical properties of the R galaxies (see also Figs. A5 and A6).

The three strongest radio galaxies, 53W032, 55W063, and 55W010, are also optically the most luminous. Although we have few new data for B galaxies, the particular case of 55W010 re-emphasizes the heterogeneity of this class.

Altogether, there are now seven spectroscopically confirmed quasars. As a class, they are of interest because of their low optical and radio fluxes.

With this supplementary list of redshifts, our survey is now spectroscopically complete to $F=19.1$.

Note added in proof: Recent ultradeep CCD photometry with the Palomar 200″ telescope in the Hercules field demonstrated that the F-magnitude zero points claimed in Sect. 2.2.2 are indeed accurate to within $0^m.15$.

References

Auriemma, C., Perola, G.C., Ekers, R.D., Fanti, R., Lari, C., Jaffe, W.J., Ulrich, M.-H.: 1977, *Astron. Astrophys.* **57**, 41

Bahcall, J.N., Soneira, R.M.: 1980, *Astrophys. J. Suppl.* **44**, 73

Bertola, F., Capaccioli, M., Oke, J.B.: 1982, *Astrophys. J.* **254**, 494

Blumenthal, G., Miley, G.K.: 1979, *Astron. Astrophys.* **80**, 13

Bruzual A., G.: 1981, *Ph. D. thesis*, Univ. of California, Berkeley

Bruzual A., G.: 1983, *Astrophys. J.* **273**, 105

Burstein, D., Heiles, C.: 1982, *Astron. J.* **87**, 1165

Heckman, T.M.: 1983, *Astrophys. J.* **268**, 628

Hummel, E.: 1980, Ph. D. thesis, Univ. of Groningen

Katgert, P., de Ruiter, H.R., van der Laan, H.: 1979, *Nature* **280**, 20

Katgert, P., Thuan, T.X., Windhorst, R.A.: 1983, *Astrophys. J.* **275**, 1

Koo, D.C.: 1981, Ph. D. thesis, Univ. of California, Berkeley

Koo, D.C., Kron, R.G.: 1982, *Astron. Astrophys.* **105**, 107

Kristian, J., Sandage, A., Westphal, J.A.: 1978, *Astrophys. J.* **221**, 383

Kron, R.G., Chiu, L.-T.G.: 1981, *Publ. Astron. Soc. Pacific* **93**, 397

van der Kruit, P.C., Allen, R.J.: 1976, *Ann. Rev. Astron. Astrophys.* **14**, 417

van der Laan, H., Windhorst, R.A.: 1982, in *Proc. of the Vatican Study Week on Cosmology and Fundamental Physics, Astrophysical Cosmology*, eds. H.A. Brück, G.V. Coyne, M.S. Longair, Vaticano: Pontificiae Academiae Scientarum, p. 263

Meier, D.L., Ulrich, M.-H., Fanti, R., Gioia, I., Lari, C.: 1979, *Astrophys. J.* **229**, 25

Meurs, E.J.A.: 1982, Ph. D. thesis, Univ. of Leiden

Mitchell, K.J.: 1983, in *Quasars and Gravitational Lenses*, 24th Liège International Astrophysical Colloquium, ed. J.P. Swings, p. 276

Oort, M.J.A., Windhorst, R.A.: 1985, *Astron. Astrophys.* (in press)

Peacock, J.A., Gull, S.F.: 1981, *Monthly Notices Roy. Astron. Soc.* **196**, 611

Robertson, J.G.: 1980, *Monthly Notices Roy. Astron. Soc.* **190**, 143

Roos, N.: 1981, Ph. D. thesis, Univ. of Leiden

Roos, N.: 1985, *Astrophys. J.* (in press)

Sandage, A.: 1973, *Astrophys. J.* **183**, 731

Tielens, A.G.G.M., Miley, G.K., Willis, A.G.: 1979, *Astron. Astrophys. Suppl.* **35**, 162

Usher, P.D., Mitchell, K.J.: 1982, *Astrophys. J. Suppl.* **49**, 27

Windhorst, R.A., Kron, R.G., Koo, D.C., Katgert, P.: 1982, in *Extragalactic Radio Sources*, IAU *Symp.* **97**, eds. D.C. Heeschen, C.M. Wade, Reidel, Dordrecht, p. 427

Windhorst, R.A., van Heerde, G.M., Katgert, P.: 1984, *Astron. Astrophys. Suppl.* **58**, 1 (Paper I)

Windhorst, R.A., Kron, R.G., Koo, D.C.: 1984, *Astron. Astrophys. Suppl.* **58**, 39 (Paper II)

Windhorst, R.A., Oppe, J.: 1984, *Astron. Astrophys. Suppl.* (submitted, Paper IV)

Windhorst, R.A., Oort, M.J.A., Katgert, P.: 1984, *Astron. Astrophys.* (submitted)

Zamorani, G., Henry, J.P., Maccacaro, T., Tananbaum, H., Soltan, A., Avni, Y., Liebert, J., Stocke, J., Strittmatter, P.A., Weymann, R.J., Smith, M.C., Condon, J.J.: *Astrophys. J.* **245**, 357

© European Southern Observatory • Provided by the NASA Astrophysics Data System